Miner Deposita (2015) 50:767–793
DOI 10.1007/s00126-015-0614-z

INVITED PAPER

Epithermal paleosurfaces

Richard H. Sillitoe[1]

Received: 24 July 2015 / Accepted: 24 August 2015 / Published online: 5 September 2015

Abstract Many active volcanic-hydrothermal and geothermal systems are characterized by distinctive surface and near-surface landforms and products, which are generated during discharge of a spectrum of fluid types under varied conditions. Remnants of most of these products are preserved in some of their less-eroded, extinct equivalents: epithermal deposits of high-sulfidation (HS), intermediate-sulfidation (IS), and low-sulfidation (LS) types. Steam-heated alteration occupying vadose zones and any underlying silicified horizons formed at paleogroundwater tables characterize HS, IS, and LS deposits as do hydrothermal eruption craters and their subaerial or shallow sub-lacustrine breccia aprons and laminated infill. Although rarely recognized, HS, IS, and LS systems can also contain finely laminated, amorphous silica sediments that accumulated in acidic lakes and mud pots and, exclusive to HS systems, in hyperacidic crater lakes. In contrast, silica sinter and more distal carbonate travertine are hot spring discharge products confined mainly to LS and IS settings, as both form from near-neutral-pH liquids. Hydrothermal chert deposition and sediment silicification can take place in shallow, lacustrine rift settings, also largely restricted to LS and IS deposits. These surface and near-surface hydrothermal products are typically metal deficient, although mercury concentrations are relatively commonplace and were formerly exploited in places. Nonetheless, sinters, hydrothermal eruption craters, and silicified lacustrine sediments may contain anomalously high precious metal values; indeed, the last of these locally constitutes low-grade, bulk-tonnage orebodies. The dynamic nature of epithermal paleosurfaces, caused by either syn-hydrothermal aggradation or degradation, can profoundly affect deposit evolution, leading to either eventual burial or telescoping of shallower over deeper alteration ± precious metal mineralization. Formational age, tectonic and climatic regime, hydrothermal silica content and texture, and post-mineralization burial history combine to determine the preservation potential of paleosurface products. Proper identification and interpretation of paleosurface products can facilitate epithermal precious metal exploration. Proximal sinters and hydrothermal eruption craters may mark sites of concealed epithermal mineralization, whereas paleogroundwater table silicification and steam-heated blankets can be more widely developed and, hence, less diagnostic. Epithermal precious metal deposits may immediately underlie paleosurface features but are commonly separated from them by up to several hundred vertical meters, especially in the case of IS deposits. Furthermore, the tops of concealed, particularly IS epithermal orebodies in any particular district, irrespective of whether or not paleosurface features are preserved, can also vary by several hundred vertical meters, thereby imposing an additional exploration challenge. Precious metal contents of paleosurface products are unreliable but nonetheless potentially useful guides to concealed deposits. However, sub-paleosurface geochemical anomalism, particularly for arsenic and antimony, may indicate proximity to subjacent ore.

Keywords Epithermal deposits · Precious metals · Paleosurfaces · Hot springs · Exploration

Editorial handling: B. Lehmann

✉ Richard H. Sillitoe
aucu@compuserve.com

[1] 27 West Hill Park, Highgate Village, London N6 6ND, UK

Introduction

Epithermal precious metal deposits form in the shallow parts of volcanic fields, including associated volcano-sedimentary basins, typically at paleodepths of <1 km. Hence, it is unsurprising that many of them are accompanied by surface and near-surface hydrothermal manifestations albeit generally devoid of economic precious metal concentrations. This fact has been appreciated for more than a century, as documented by numerous early discussions of likely relationships between epithermal deposits and hot spring activity (e.g., Lindgren 1933; Schmitt 1950; White 1955). Although the genesis of epithermal deposits can be geologically brief, perhaps as little as a few tens of thousands of years (Simmons and Brown 2006; Rowland and Simmons 2012), the volcanic and/or sedimentary land surfaces overlying the deposits at the time of formation are commonly dynamic and can undergo appreciable change, thereby profoundly influencing their surface and near-surface manifestations and even formational history.

Epithermal deposits are commonly subdivided into high-sulfidation (HS), intermediate-sulfidation (IS), and low-sulfidation (LS) end-member types on the basis of their mineralogic characteristics (Hedenquist et al. 2000; Sillitoe and Hedenquist 2003; Table 1), although it is recognized that mineralogic evolution and complexity make it difficult to neatly fit some deposits into this end-member classification scheme. These three epithermal types also tend to occupy distinct volcano-sedimentary settings, characterized by different hydrologic regimes (Henley and Ellis 1983). The HS deposits typify andesitic to dacitic volcanic edifices—stratovolcanoes, dome complexes, and any associated maar volcanoes and underlying diatremes (Sillitoe and Bonham 1984), commonly in the shallow parts of porphyry copper systems—whereas LS deposits are characteristic of rift settings in which bimodal (basalt-rhyolite) volcanism and fluvio-lacustrine sedimentation are commonplace (Sillitoe 1993; Sillitoe and Hedenquist 2003). The IS deposits, mineralogically intermediate between the HS and LS types, can form in either volcanic centers or volcano-tectonic rifts. Both HS and IS deposits and LS and IS deposits can be closely associated and even transitional to one another (Sillitoe 1999; Hedenquist et al. 2000; Sillitoe and Hedenquist 2003; Camprubí and Albinson 2007), whereas HS and LS deposits normally appear to be incompatible. Epithermal deposits of LS and, to a much lesser extent, IS type in close proximity to remanent paleosurface features were initially assigned to a separate hot spring category (e.g., Berger and Eimon 1983; Nelson 1988), but are now generally treated as the shallowly formed parts of standard epithermal systems (Hedenquist et al. 2000).

In this practically oriented overview, the well-known surface manifestations of active hydrothermal systems (e.g., Hochstein and Browne 2000) are briefly summarized first in order to provide present-day analogues for epithermal paleosurface features. The principal paleosurface features associated with HS, IS, and LS epithermal deposits are then described and discussed in their overall volcanic and geomorphologic contexts (Table 2). Particular emphasis is placed on the resultant hydrothermal products and their origins—using detailed studies of active analogues wherever possible, any associated metal and metalloid anomalism, consequences for deposit-scale evolution, and preservation potential. Finally, a number of exploration implications and issues are considered.

Paleosurface features, as discussed herein, comprise hydrothermal landforms and associated surface accumulations as well as hydrothermal alteration zones generated between paleosurfaces and underlying paleogroundwater tables. In active epithermal systems, pressure gradients are controlled by the hydrostatic head that, in turn, is determined by the groundwater table or piezometric surface (Fournier 1983; Henley 1985; Simmons 2002). The distance between paleosurfaces and paleogroundwater tables is variable, ranging from close to zero in low-relief areas to as much as several hundred meters in steep terrain, especially where arid climatic conditions prevail. The alteration contributions of supergene weathering, also controlled by paleo- and present-day groundwater tables, are largely excluded from this overview, although it is recognized that hypogene and supergene processes can be transitional in the shallow epithermal environment and, in places, difficult to separate unambiguously.

Table 1 Summary characteristics of epithermal deposit types

Epithermal type	High-sulfidation (HS)	Intermediate-sulfidation (IS)	Low-sulfidation (LS)
Main mineralization styles	Steep and shallowly inclined replacement bodies, hydrothermal breccias	Veins, stockworks	Veins, stockworks, disseminated bodies
Main proximal alteration types	Silicification, vuggy residual quartz, quartz-alunite	Silicification, quartz-sericite/illite	Silicification, quartz-adularia-illite
Main gangue minerals	Quartz, alunite, barite	Quartz, calcite, manganoan carbonates, rhodonite, adularia	Quartz, chalcedony, adularia
Sulfide abundance	High (10–80 vol.%)	Moderate (5–30 vol.%)	Low (1–5 vol.%)
Sulfidation-state indicators	Enargite/luzonite/famatinite	Tetrahedrite, chalcopyrite, low-Fe sphalerite	Pyrrhotite, arsenopyrite, high-Fe sphalerite
Typical metal signature	Au-Ag-Cu ± Bi ± Te	Ag-Au-Zn-Pb-Mn ± Cu	Au ± Ag ± Se ± Mo

Summarized from Einaudi et al. (2003), Sillitoe and Hedenquist (2003)

Table 2 Summary characteristics of epithermal paleosurface features

Paleosurface feature	Associated epithermal deposit type	Proximity to hydrothermal upflow zone	Hydrothermal fluid responsible	Main component mineral(s)
Steam-heated zones	HS, IS, LS	Proximal but widespread	H_2S-bearing steam condensate	Opal/chalcedony, alunite, kaolinite, smectite
Groundwater table silicification	HS, IS, LS	Proximal but widespread	H_2S-bearing steam condensate	Opal/chalcedony
Lacustrine amorphous silica sediments	HS, IS, LS	Commonly proximal	H_2S-bearing steam and SO_2- and HCl-bearing magmatic condensates	Opal, cristobalite
Hydrothermal eruption craters and breccias	HS, IS, LS	Commonly proximal	Neutral-pH chloride water	Illite, smectite
Hot spring sinter	IS, LS	Commonly proximal	Neutral-pH chloride water	Opal/chalcedony
Hot spring travertine	IS, LS	Distal	CO_2-rich water	Calcite, aragonite
Hydrothermal chert	IS, LS	Proximal-to-distal	Neutral-pH chloride water	Opal/chalcedony
Silicified lacustrine sediments	IS, LS	Proximal-to-distal	Neutral-pH chloride water	Opal/chalcedony

Taken from references cited in the text and personal observations

Active hydrothermal systems

Active hydrothermal systems, some exploited as power sources, are sites of convective and lesser conductive dissipation of heat energy, and many of them are manifested at surface by one or more types of fluid discharge. This gives rise to a variety of distinctive landforms and products, which can be partially preserved in shallowly eroded epithermal precious metal deposits, as discussed further in the following sections.

For the purposes of the following discussion, two end-member types of high-temperature hydrothermal systems may be recognized: volcanic-hydrothermal and geothermal, with the latter subdivided into those associated with high-relief, volcanic and low-relief, rift settings (Henley and Ellis 1983; Hedenquist and Arribas 1999; Hedenquist et al. 2000; Hochstein and Browne 2000; Simmons et al. 2005; Fig. 1). In general, volcanic-hydrothermal systems can generate HS and IS epithermal mineralization, whereas geothermal systems are the sites of IS and LS mineralization.

On the summits and upper slopes of volcanic edifices overlying volcanic-hydrothermal systems, magmatic water vapor with SO_2, HCl, CO_2, and H_2S gases discharges directly to the atmosphere via high-temperature solfataras and fumaroles (Fig. 2a). Condensation of the vapor and its contained gases into groundwater produces highly acidic (pH $\leq$1) and corrosive waters, which can be ponded in hyperacidic crater lakes and mud pots and emitted from hot springs (Hedenquist 1995; Fig. 1a). Warm and cold springs, both acidic and neutral pH, can debouch on the lower volcano slopes, up to ~10 km from the summits (e.g., Giggenbach et al. 1990; Fig. 1a).

Geothermal systems are characterized by relatively reduced, neutral-pH, alkali chloride waters, although the magmatic component can still be appreciable (e.g., Sillitoe and Hedenquist 2003), particularly where systems are developed beneath high-relief volcanic centers. In such situations, the deeper, neutral-pH water fails to attain the surface at the higher elevations and steam separated from the boiling liquid at depth dominates and gives rise to surficial steam-heated features, including fumaroles, mud pots, and steaming ground (Fig. 2b) as well as outflow of acidic water (Fig. 1b). Discharging acidic water can also accumulate in shallow lakes, some occupying hydrothermal eruption craters. The low-pH (~2–3), acid-sulfate water responsible for the steam-heated alteration results from groundwater absorption of H_2S-bearing steam derived from boiling of the deeper, neutral-pH geothermal water (White et al. 1956; White 1967; Schoen 1969; Schoen et al. 1974). Lateral flow of both the steam-heated and underlying alkali chloride waters, the latter for distances as great as ~10 km, is accompanied by CO_2-rich marginal water (Hedenquist 1990), which becomes bicarbonate dominated as CO_2 is lost by effervescence. Distal springs discharge groundwater-diluted chloride, bicarbonate, or hybrid bicarbonate-sulfate waters capable of precipitating silica sinter if not too dilute and cool, with the bicarbonate waters also forming travertine, surficial carbonate accumulations (Fig. 1b).

In marked contrast, geothermal systems hosted within low-relief terrain commonly discharge neutral-pH, alkali chloride waters along streams and on lake margins and bottoms, although shallow boiling also gives rise to nearby steam-heated features above the groundwater table (Fig. 1c). The discharging alkali chloride waters, which can be channeled by the breccia conduits beneath hydrothermal eruption craters, typically form silica sinters (Fig. 1c). The active steam-heated environment is characterized by the same hydrothermal features observed in high-relief geothermal systems (Fig. 2b). The peripheral parts of these low-relief geothermal systems

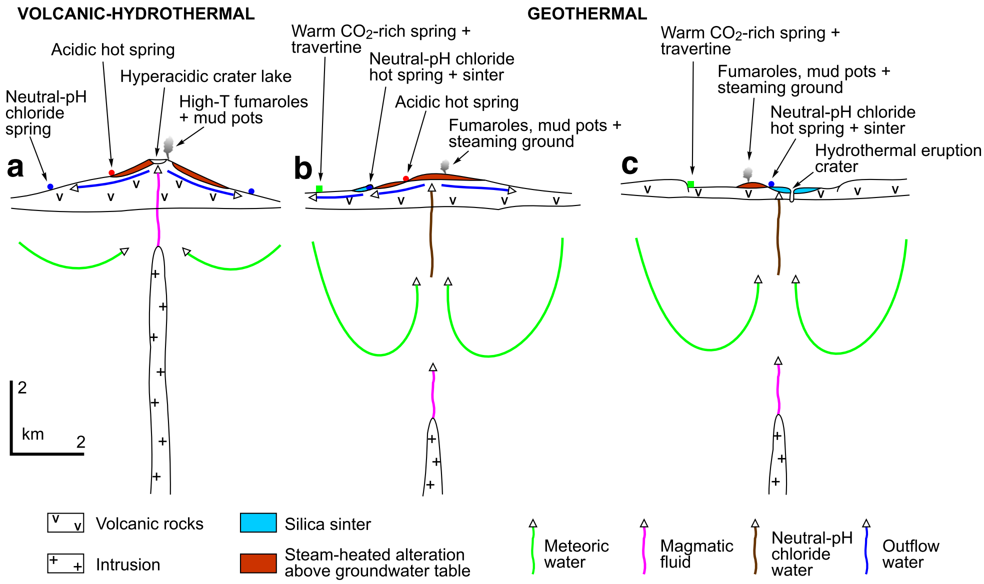

Fig. 1 Schematic representation of active, high-temperature hydrothermal systems and their principal surface features (inspired by Hedenquist and Arribas 1999; Hochstein and Browne 2000; Simmons et al. 2005). **a** Volcanic-hydrothermal system above shallow intrusion and dominated by magmatic fluids. **b** Geothermal system above deep intrusion in high-relief terrain, with ascendant neutral-pH, alkali chloride water unable to attain the surface except in outflow zones. **c** Geothermal system above deep intrusion in low-relief terrain, with deep neutral-pH, alkali chloride water reaching the surface. Note that steam-heated alteration above groundwater tables is far less extensive in **c** than in **a** or **b**

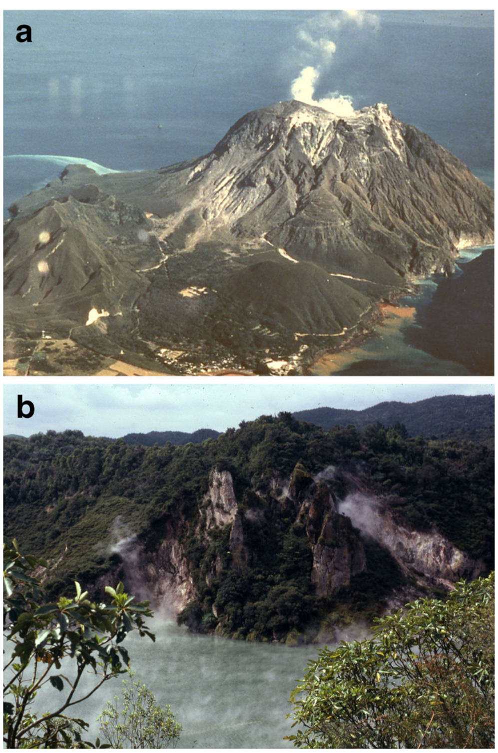

Fig. 2 Contrasting surface discharges from active systems. **a** Magmatic volatiles, rich in SO_2 and HCl, passively discharging at temperatures of 800–900 °C from a volcanic-hydrothermal system at the Satsuma-Iwojima volcano, a rhyolite dome in Kyushu, Japan (see Hedenquist et al. 1994; Kazahaya et al. 2002). **b** Steaming ground at Cathedral Rocks above a paleogroundwater table represented by the level of Frying Pan Lake (6-m deep, pH 3.5, 55 °C), Waimangu geothermal system, Taupo Volcanic Zone, North Island, New Zealand (see Simmons et al. 1993)

also tend to be dominated by weakly acidic, CO_2-rich waters, which can precipitate travertine on surface discharge (Fig. 1c).

Epithermal paleosurface products

Steam-heated zones

The reactive H_2S-bearing steam condensate formed in the vadose zone above groundwater tables causes advanced argillic alteration (Fig. 3) and, in poorly consolidated volcanic material, can produce near-surface cavities (Fig. 4a) and resultant collapse features. At the prevailing low (<~120 °C) temperatures, the advanced argillic assemblage comprises powdery opaline silica, alunite, and/or kaolinite (Fig. 4b), depending on solution pH. The opaline silica, which is diagenetically transformed to microcrystalline quartz (chalcedony; White et al. 1956), forms at pH 2–3, whereas kaolinite and more distal smectite characterize rock volumes subjected to less-acidic conditions (Fig. 3). Minor disseminated pyrite can occur in the proximal portions of steam-heated blankets, but it tends to be promptly oxidized as the foci of steam emission migrate. Steam-heated alteration is everywhere characterized by its low density, typically <2. Actively forming steam-heated zones, like that capping part of the Ladolam LS gold deposit, Lihir Island, Papua New Guinea, are represented at surface by steaming ground and corresponding vegetation-kill zones (Carman 2003; Fig. 2b).

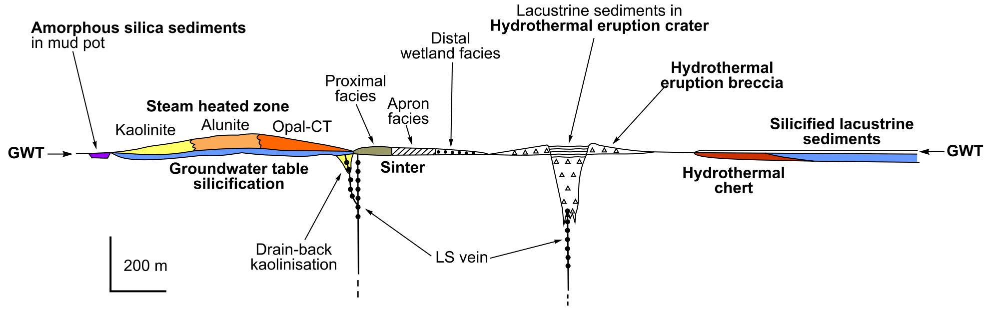

Fig. 3 Schematic relationships between a steam-heated zone, lacustrine amorphous silica sediments, groundwater table silicification, silica sinter, hydrothermal eruption crater and breccia, hydrothermal chert, and silicified lacustrine sediments. Note the pH-controlled mineralogic zoning of the steam-heated zone, temperature-controlled proximal-to-distal zoning of the sinter, and sub-groundwater table kaolinization caused by drain-back of acidic water. *GWT* groundwater table

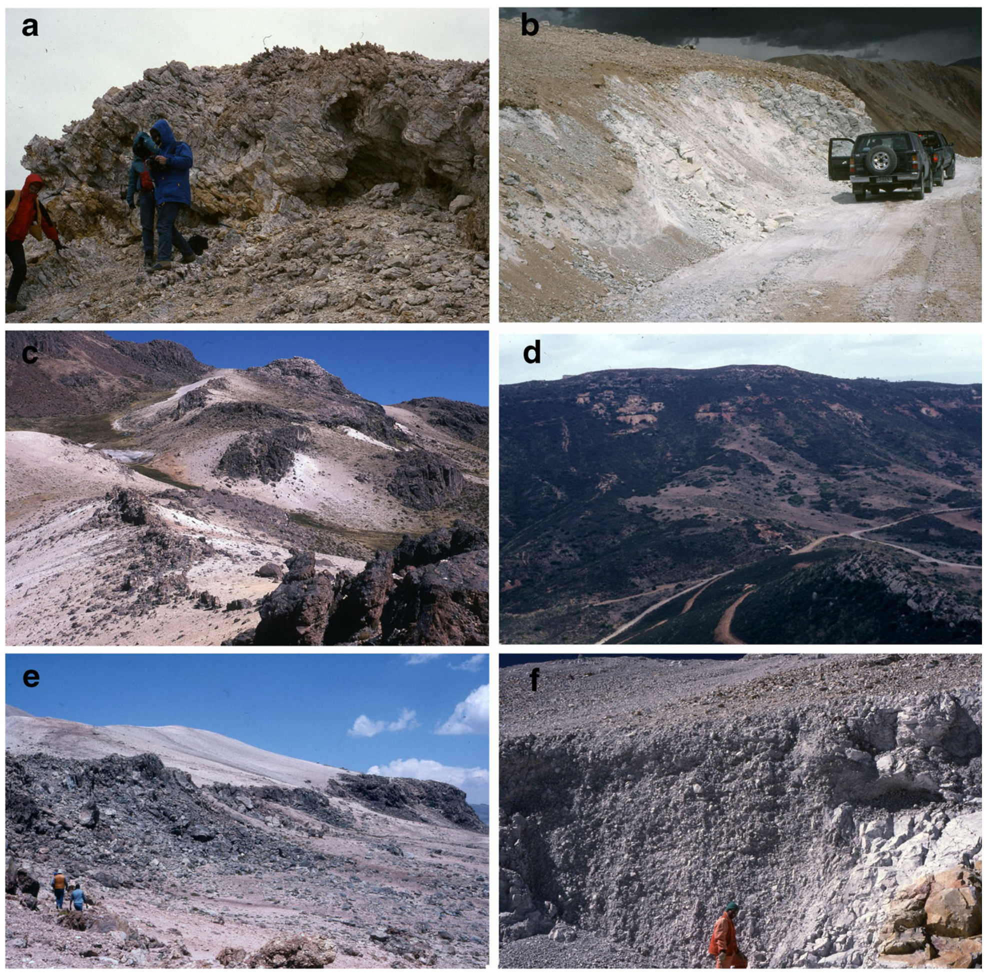

Fig. 4 Images of steam-heated alteration and paleogroundwater table silicification. **a** Cavity produced by rock dissolution in steam-heated remnant above the advanced argillic lithocap of the Marte porphyry gold deposit, northern Chile (see Sillitoe 1994). **b** Steam-heated alteration exposed in a road cut above the Coipa Norte HS gold-silver orebody at La Coipa, northern Chile. Note its white, friable character. **c** Steam-heated alteration around the outcropping, weakly mineralized upper part of the Tres Reyes vein at the Arcata IS silver deposit, Peru (see Candiotti et al. 1990). **d** Subhorizontal zone of paleogroundwater table silicification (forming the present surface) alongside the Furtei HS gold deposit, Sardinia, Italy. Note the formerly exploited kaolinite quarries beneath the silicified horizon. The kaolinization was generated by drain-back of acidic water from an overlying, but now-eroded steam-heated zone. **e** Subhorizontal zone of paleogroundwater table silicification and overlying steam-heated alteration peripheral to the La Coipa HS-IS gold-silver district, Chile. **f** Hydrothermal breccia, generated by shallow-seated steam eruption, cutting steam-heated zone, Pascua-Lama HS gold-silver deposit, Chile. Geologist stands just left of contact with non-brecciated rocks

Since boiling of ascendant fluids and upward liberation of H_2S-bearing steam are features of all types of epithermal systems, HS, IS, and LS deposits can be capped by steam-heated zones (Sillitoe 1993; Hedenquist et al. 2000). These blankets are essentially indistinguishable from one another because the acidic solutions and, hence, the resultant minerals are essentially the same in all cases. Steam-heated zones above many HS and some IS deposits tend to be thicker than those above LS deposits because groundwater tables are typically deeper in high-relief volcanic edifices than in topographically subdued rift settings. Indeed, LS deposits may be characterized by only thin veneers of steam-heated alteration or may lack it entirely as, for instance, in lacustrine settings (Fig. 3). Since the thickness of steam-heated zones is influenced by the depth of groundwater tables, they also tend to be thicker where prevailing climatic regimes are arid rather than pluvial. Aridity also decreases groundwater recharge and consequent dilution, thereby allowing buildup of the steam condensate. The anoxic atmosphere during the Archean precluded steam-heated alteration because the liberated H_2S would have remained unoxidized, as exemplified by the North Pole epithermal system, Western Australia (Harris et al. 2009).

Native sulfur, a product of H_2S oxidation by atmospheric oxygen under acidic conditions, is widespread in steam-heated zones but tends to be more abundant in those developed at the tops of HS systems, from which it was formerly exploited in places (e.g., La Coipa, Chile; El Queva, Argentina; Sillitoe 1975). However, much of the native sulfur (± iron sulfides) at the tops of HS systems, like that formerly exploited from the summit regions of some andesitic-dacitic arc volcanoes (e.g., Aucanquilcha, Chile; Matsuo, Honshu, Japan; White Island, New Zealand) and still mined in artisanal fashion at Kawah Ijen, Java, Indonesia, was probably more commonly deposited from solfataras fed directly by magmatic gas with variable SO_2/H_2S ratios (Mukaiyama 1970; Giggenbach 1987). Temperature rise (>~115 °C) and consequent fusion of such solfataric sulfur accumulations can lead to sulfur pools and flows (Watanabe 1940; Naranjo 1985; Oppenheimer 1992).

Steam-heated alteration generally constitutes areally extensive blankets, remnants of which are still observed at many epithermal precious metal deposits of HS (e.g., Yanacocha, Peru, Veladero, Argentina, and Pascua-Lama, Chile-Argentina; Harvey et al. 1999; Deyell et al. 2005), IS (Arcata, Peru; Candiotti et al. 1990), and LS types (Wind Mountain, Hycroft [Crowfoot-Lewis], and Florida Canyon, Nevada; Wood 1991; Ebert and Rye 1997; Fifarek et al. 2010). However, the basal remnants of steam-heated zones can have upward-flared, funnel-shaped geometries centered on individual veins, vuggy residual quartz ribs, faults, or fracture zones (e.g., Arcata; Fig. 4c).

Kaolinite alteration is commonly observed as root zones of steam-heated blankets, either as laterally extensive but vertically restricted zones (Fig. 3) or alongside the shallow parts of LS and IS veins. The kaolinite can also line or fill open spaces in the veins themselves. Although this kaolinization can be formed by descent of groundwater tables, it is also due to permeability-controlled, commonly structurally guided drain-back of steam-heated waters, probably as the epithermal systems waned. Kaolinite of this type, beneath paleogroundwater table silicification, was formerly exploited alongside the Furtei HS gold deposit in Sardinia, Italy (Fig. 4d). At Mt. Muro in Central Kalimantan, Indonesia, late-stage kaolinite developed alongside and within some of the auriferous veins as the IS system waned (Simmons and Browne 1990).

Groundwater table silicification

The groundwater table, marking the subhorizontal bases of steam-heated zones, can undergo massive silicification (Sillitoe 1993; Hedenquist et al. 2000). The silicified zones range from a few to several tens of meters in thickness and are normally subhorizontal unless subjected to later tilting (Figs. 3 and 4d, e). The silica is initially precipitated as replacement opal, but progressively transforms to chalcedony as a result of recrystallization. Limonite impregnation and staining developed by supergene oxidation of pyrite ± marcasite are commonplace.

Much of the silica precipitated at groundwater tables is dissolved in the vadose zone by steam condensate, typically from volcanic glass contained in tuffs. The condensate flows laterally at the groundwater table or within perched aquifers, following local hydraulic gradients. This implies the likelihood of greater silica transport and deposition, at distances up to several kilometers, in high-relief areas than in rifts or other topographically subdued volcanic settings. The silicified horizons are commonly hydrothermally brecciated, with the clasts variably re-cemented by opaline silica or derivative chalcedony. The brecciation is attributed to sealing of the impermeable silicified horizons and eventual buildup of pressures and rupturing to form shallow-seated steam eruptions, which can also cause brecciation of overlying steam-heated blankets (Mongillo and Allis 1988; Fig. 4f).

In several epithermal districts, groundwater table silicification can be traced for several kilometers along their apparent margins, although it has been largely eroded or simply never formed above most of the known orebodies, as observed near the Furtei HS gold deposit (Fig. 4d), in the La Coipa HS-IS gold-silver district (Fig. 4e), in the Fresnillo IS silver district, Mexico (Albinson 1988; Sawkins 1988), and in the Goldbanks LS gold district, Nevada (Stone et al. 2000; Ellis and Stroup 2015). At the Hycroft gold deposit, an opaline silica (opalite) horizon, up to 12-m thick, underlies the extensive steam-heated blanket (Ebert and Rye 1997).

Lacustrine amorphous silica sediments

Acidic lakes and mud pots can exist in HS, IS, and LS systems where the acidity is typically due to absorption of boiled-off, H_2S-bearing steam by standing water. However, magmatic condensate, produced by direct input of SO_2, HCl, and H_2S from underlying, high-level magma chambers is dominant in the HS environment, most notably in hyperacidic (pH≤1) crater lakes, such as those perched high on the Ruapehu, North Island, New Zealand, Poás, Costa Rica, and Kawah Ijen composite volcanoes (e.g., Rowe et al. 1992; Christenson and Wood 1993; Delmelle and Bernard 1994), as well as some lakes within volcanic dome complexes. Hyperacidic crater lakes are considered to overlie potential sites of HS epithermal ore deposition (Hedenquist 1995).

Sediments suspended in the water columns and accumulating on the floors of these acidic lakes and mud pots are dominated by fine-grained opal-CT and opal-C (cristobalite) along with one or more of gypsum, barite, anatase, native sulfur, and pyrite: the ultimate products of rock dissolution by hot, low-pH fluids (Brantley et al. 1987; Delmelle and Bernard 1994; Hedenquist and Taran 2013). The so-called silica residue, described by Rodgers et al. (2002, 2004), is a similar, small-volume product that accumulates in acidic pools and mud pots in the LS geothermal systems of the Taupo Volcanic Zone, North Island, New Zealand. Alunite and kaolinite can also accumulate as sediments in somewhat less-acidic lakes and mud pots. The amorphous silica-dominated sediments are typically finely laminated (Fig. 5a) and can display soft-sediment deformation features, some caused by material sloughed from steep and unstable lake margins. Native sulfur occurs as molten accumulations on the floors of some acidic lakes and is present locally as interbeds and impregnations in the chemical sediments (Kusakabe et al. 1986; Delmelle and Bernard 1994; Fig. 5a).

These amorphous silica sediments have not been widely recognized in epithermal deposits, and crater lake sediments appear to be unknown. Nonetheless, several remanent patches of chemical sediments of this type abut the advanced argillic-altered dacitic domes at the Yanacocha gold deposit (JW Hedenquist, written commun, 2015) and elsewhere, although in some places they may be difficult to distinguish from lacustrine sediments that have been subjected to intense steam-heated alteration and, hence, are dominated by opaline silica.

Hydrothermal eruption craters and breccias

Hydrothermal eruption craters are most readily recognized by the localized presence of lacustrine mudstones and/or the crudely bedded breccia aprons that surround them. The breccias are commonly polymictic, poorly sorted, angular to subangular, and matrix supported (Fig. 5c); can contain clasts of surface and subsurface hydrothermal products, such as sinter and epithermal vein material in IS and LS systems; and lack juvenile magmatic components. The craters themselves can range in size from several (Fig. 5b) to hundreds of meters and are generally filled by laminated sediments, ranging in composition from amorphous silica in hot, acidic lakes to mudstones in cold lakes. The largest of ten Holocene craters beneath and alongside Lake Rotokawa in the Taupo Volcanic Zone is ~1.5 km in diameter (Krupp and Seward 1987). In the case of large eruptions, the breccia aprons can extend for up to ~2 km outboard of the craters, and sub-crater brecciation can extend downward for several hundred meters (Collar and Browne 1985; Hedenquist and Henley 1985). Nonetheless, distinction between amorphous silica sediments

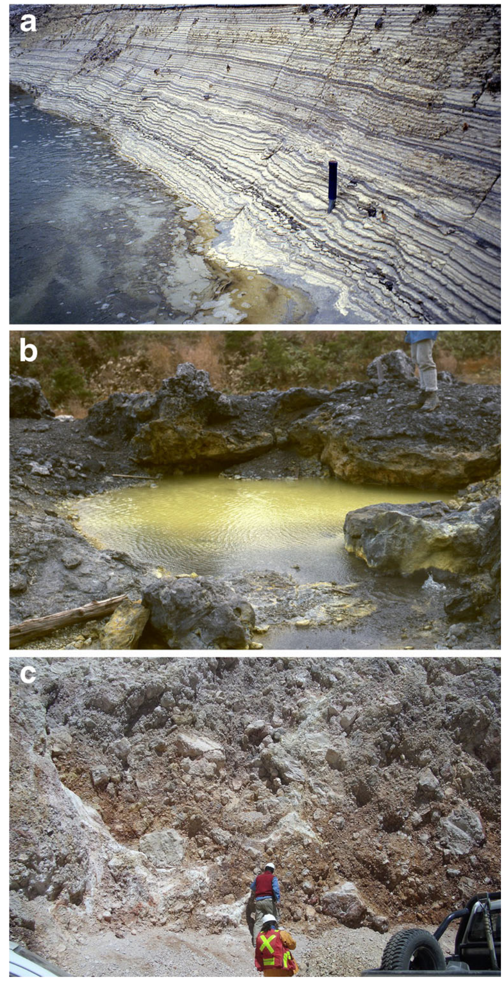

Fig. 5 Images of lacustrine amorphous silica sediments and hydrothermal eruption breccias. **a** Finely laminated, lacustrine amorphous silica sediments in the breached crater lake at Jogoku-dani in the Tateyama volcano, Honshu, Japan (see Kusakabe et al. 1986). Yellow coloration of certain layers is due to native sulfur impregnation. **b** Small hydrothermal eruption crater filled with boiling water and surrounded by eruption breccia composed of black mudstone clasts, Osorezan, Honshu, Japan (see Aoki 1992). Note the yellow color of the water due to amorphous arsenic sulfide flocculent. **c** Crudely bedded, polymictic, hydrothermal eruption breccia above the Pascua-Lama HS disseminated gold-silver deposit, Chile

filling a small hydrothermal eruption crater that has lost its breccia apron to erosion from those deposited in a mud pot or other restricted depression is nigh impossible.

Hydrothermal eruptions are commonly caused by rapid subsurface buildups of fluid pressure, transferred from depth via a non-condensable gas phase (Hedenquist and Henley 1985), sometimes beneath impermeable barriers (Fournier 1983, 1985; Hedenquist and Henley 1985; Nelson and Giles 1985) but commonly without such impediments (Browne and Lawless 2001). However, external triggers such as faulting, lake drainage, seismic activity, and/or magma intrusion contributing CO_2, as in the case of the Waiotapu geothermal system in the Taupo Volcanic Zone (Nairn et al. 2005), can also play important roles.

A series of Holocene hydrothermal eruption craters formed under shallow-water conditions near the shore of the caldera lake at Osorezan, Honshu, Japan, with one of them still filled by H_2S-rich, neutral-pH, boiling chloride water that is actively depositing sulfur, orpiment, and gold (Aoki and Thompson 1990; Izawa and Aoki 1991; Aoki 1992; Fig. 5b). A sub-lacustrine, bedded native sulfur deposit formed in the largest hydrothermal eruption crater at Lake Rotokawa as a result of bacteriogenic oxidation of H_2S (Krupp and Seward 1987). Hydrothermal eruption craters and associated breccia remnants mark epithermal paleosurfaces at several localities, and the breccias are particularly widespread at the Hycroft LS (Ebert and Rye 1997) and Pascua-Lama HS deposits (Fig. 5c). The breccias may be interbedded with sinter at LS deposits, as at McLaughlin, California (Lehrman 1986), and Milestone in the Silver City district, Oregon (Rytuba and Vander Meulen 1991b). The same situation is represented by the siliceous breccia capping Bodie Bluff in the Bodie LS gold district, California, and the breccia above the Golden Promise LS gold vein in the Republic district, Washington, which both contain sinter and LS vein fragments (Silberman and Chesterman 1991; Fifarek et al. 1996). The hydrothermal eruption crater that once overlay much of the blind Favona LS vein gold deposit in the Waihi district, North Island, New Zealand, was at least 800-m long and 300-m wide, judging by the size of the underlying vent breccia, which also contains both sinter and vein clasts (Torckler et al. 2006; Fig. 6). The localized, inward-thickening mudstone sequence that overlies the Yamada LS vein system at Hishikari, Kyushu, Japan, is also interpreted as a hydrothermal eruption crater, although any associated breccia deposits have been eroded (Izawa et al. 1993). A similar situation is described from the Broken Hills LS gold-silver deposit, North Island, New Zealand (Rabone 2006).

Hot spring sinter

Silica sinter forms aprons or terraces where hot (≤100 °C), ascendant, near-neutral-pH, amorphous silica-saturated fluids

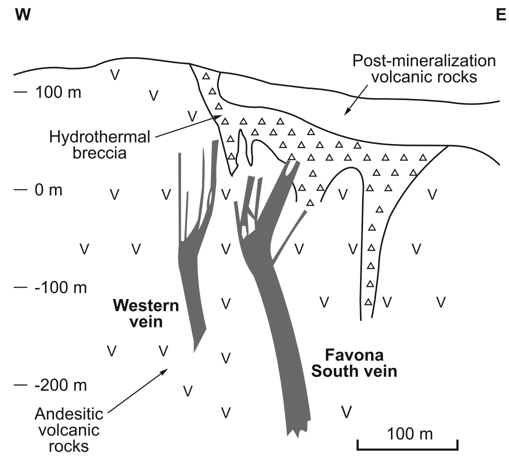

Fig. 6 Section showing the spatial relationship between the top of the geologically blind LS epithermal veins and hydrothermal breccia filling the vent below a now-eroded eruption crater at the Favona LS gold-silver deposit, Waihi district, North Island, New Zealand (taken from Mauk et al. 2006)

discharge at the surface (Fig. 3), a situation that is only possible where groundwater tables intersect the surface as, for example, along lake shores or river banks; hence, the widespread association of sinter with lacustrine and fluvial sedimentary strata (e.g., Rytuba and Vander Meulen 1991a; Yahata et al. 1994; Wallace et al. 2008). Sinter also forms mounds around geyser vents, which can be marked by chimney-like silica constructions attaining heights of up to several meters (Fig. 7a). Sinter and steam-heated alteration can occur nearby one another and may be considered as lateral equivalents (Fig. 3). Amorphous silica, opal-A, is precipitated as the hot water flows across the discharge aprons or down the terraces, with distinctive pool sinter forming where the water ponds (Fig. 7b). Microbial activity besides cooling and evaporation plays a prominent role in sinter formation (e.g., Jones et al. 2001). The presence of amorphous silica sinter indicates subsurface reservoir temperatures in excess of ~200 °C, assuming the liquid is saturated with quartz (White 1973; Fournier 1985).

The non-crystalline opal-A transforms through poorly crystalline opal-CT and opal-C to moganite (monoclinic silica) and then microcrystalline quartz (chalcedony) in ~50, 000 years, with a concomitant increase in density, decrease in both water content and porosity, and destruction of microtextures (White et al. 1988; Herdianita et al. 2000; Rodgers et al. 2004; Lynne et al. 2007). Hence, epithermal sinters, typically Pliocene or older, are predominantly composed of chalcedony. The aging process appears to be accelerated by the presence of organic and other impurities, elevated depositional and post-depositional temperatures, and post-depositional burial (Herdianita et al. 2000).

Most sinter accumulations are associated with LS epithermal deposits because it is the epithermal type that forms

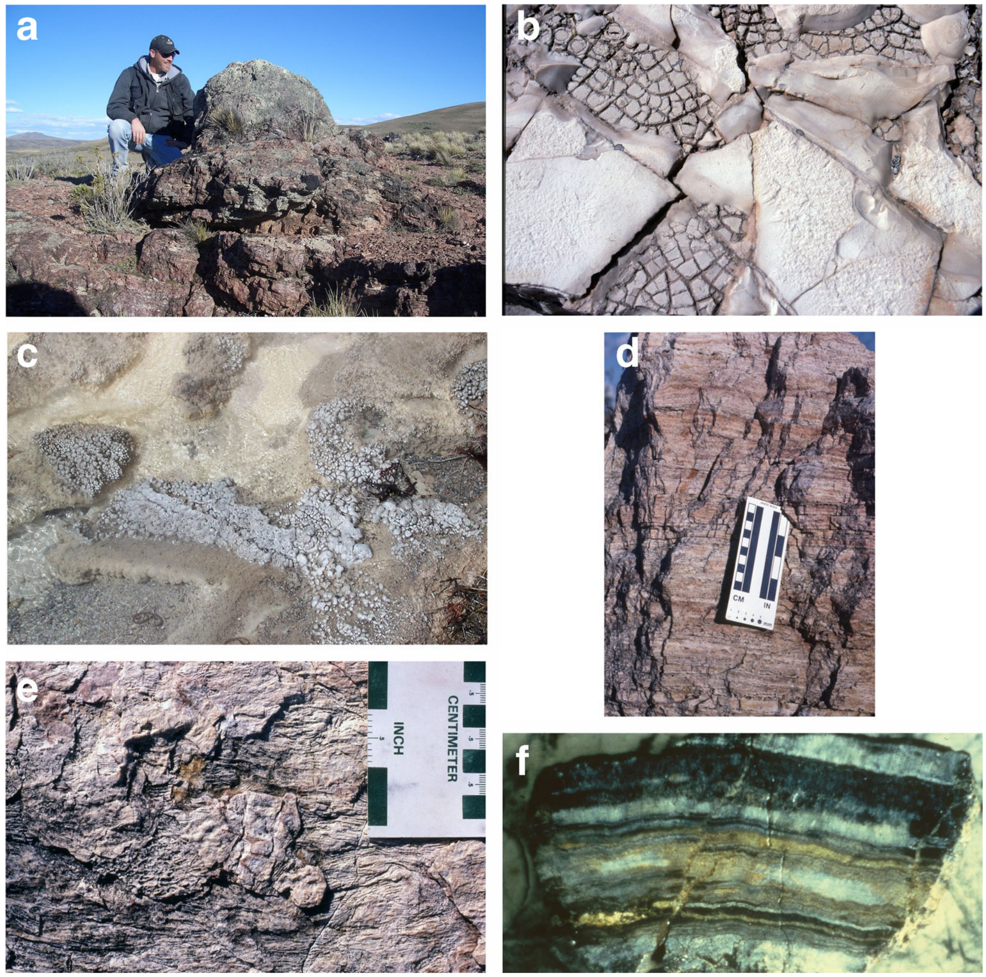

Fig. 7 Images of hot spring sinter and travertine. **a** Geyser vent mound at the southeastern extremity of the Cerro Negro vein system, Deseado massif, Patagonia, Argentina. **b** Pool sinter displaying syneresis cracks, Milos island, Greece. Image is ~40 cm across. **c** Geyserite from Orakeikorako geothermal system, Taupo Volcanic Zone, North Island, New Zealand. Image is ~20 cm across. **d** Chalcedonic sinter with bedding-parallel cavities (bubble-mat texture), Verbena, Drummond Basin, Queensland, Australia. **e** Silicified filamentous bacterial streamer fabric on bedding plane of chalcedonic sinter indicative of direction of water flow over sinter apron, Verbena, Drummond Basin, Queensland, Australia. **f** Travertine, showing layering and manganese and iron staining, Wau IS gold district, Papua New Guinea. Image is ~40 cm across

in rift settings where outcropping groundwater tables are more likely (Sillitoe and Hedenquist 2003). However, some IS epithermal systems generated in pull-apart rift basins also include sinter, as exemplified by Fruta del Norte, Ecuador (Leary et al. 2007). In contrast, there are no well-authenticated examples of sinter associated with HS epithermal deposits, probably for the simple reason that it does not form because silica polymerization and precipitation are inhibited in acidic (pH <3–4) fluids, typical of HS systems (Fournier 1985). Nonetheless, as described above, amorphous silica does form colloids that accumulate as finely laminated sediments in acidic lakes.

Sinter recrystallized to chalcedony is normally distinguishable by its non-planar, finely laminated or banded texture (Fig. 7d) and multi-colored (white, yellow, green, tan, red-brown, gray, and/or black) character, typically ascribed to iron, manganese, and mercury impurities. Also diagnostic is the presence of columnar microbial structures perpendicular to the laminae (coniform texture); irregular, lenticular cavities parallel to the laminae (bubble-mat texture; Fig. 7d); nodular and other forms of geyserite formed in evaporative splash zones of geysers (Fig. 7c); filamentous microbial forms occurring as bedding-parallel streamers indicative of water flow direction (Fig. 7e); oncoids that grow in turbulent pools; and/or plant root, stem, and leaf molds in both growth and flow-aligned positions; as well as other textures (e.g., Lynne 2012). Nonetheless, in float or drill core and where rock outcrop is poor, sinter that is recrystallized to chalcedony and underwent additional silica introduction can sometimes be tricky to tell apart from colloform-banded LS epithermal vein chalcedony.

In reasonably well-preserved sinter occurrences, a series of depositional environments may be defined, from proximal, high-temperature (>70 °C), near-vent zones typified by various types of abiotic geyserite, through mid-slope aprons, terraces, and pools characterized by stromatolitic growth and thermophilic bacterial mats, to distal, cool (<35 °C), and plant-rich wetland (marsh) facies (e.g., Walter et al. 1996; Lynne 2012; Channing and Edwards 2013; Fig. 3). Syn- or post-depositional erosion of sinter aprons and terraces results in clastic facies (e.g., Steamboat Springs, Nevada; White et al. 1964). Sinter can commonly be interbedded with fluvial, lacustrine, or volcaniclastic material, which itself may undergo complete or partial silicification (e.g., White et al. 1964; Campbell et al. 2003). A variety of biota, including stromatolites, filamentous microbes, diatoms, and plants, has been described in detail from several sinters, ranging in age from Paleozoic (Trewin 1993; Walter et al. 1998) through Jurassic (Guido et al. 2010) to Recent (Jones et al. 2001), although their preservation potential tends to decrease progressively with increasing age (de Wet and Davis 2010).

Several LS epithermal gold-silver deposits occur beneath or alongside contemporaneous siliceous sinter remnants, including steep vein systems at National and Fire Creek, Nevada (Vikre 1987; Milliard et al. 2015), McLaughlin (Lehrman 1986), Cerro Blanco, Guatemala (White et al. 2010), and El Dorado, El Salvador (Richer et al. 2009); disseminated mineralization and deeper bonanza-grade veins at Ivanhoe, Nevada (Wallace 2003); and, as far as is known, disseminated mineralization alone at Hasbrouck Mountain and Buckhorn, Nevada (Graney 1987; Jennings 1991). At all these localities, the sinter is underlain by and/or interbedded with lacustrine sedimentary and volcaniclastic rocks that were also partially silicified and subjected locally to steam-heated alteration. The major Cerro Vanguardia LS vein gold deposit in the Late Jurassic Deseado massif of Patagonia, Argentina, was also likely generated beneath a fluvio-lacustrine setting and can be traced along strike into extensive areas of preserved paleosurface features, including proximal-to-distal sinter accumulations (Guido and Campbell 2014).

Hot spring travertine

Travertine aprons or terraces are constructed as a result of CO_2 degassing where relatively low-temperature, CO_2-rich waters attain the surface. As in the case of sinter, this is typically where the groundwater table intersects the surface. However, since sinter and travertine are the products of completely different chemical processes, as discussed earlier, they are not normally closely associated in epithermal systems (Fig. 3); however, modern-day exceptions are known (Campbell et al. 2002; Smith et al. 2011). Travertines are commonly fed via extensional faults and fractures marked by fissure-ridge deposits: outwardly dipping, bedded travertine flanking fissures filled by vertically banded travertine; however, tufa cones form where the controlling fissures underlie unconsolidated sediments, as on lake floors (Hancock et al. 1999).

Travertine is characterized by a variety of facies, ranging from micritic to coarsely crystalline and from hard and dense (Fig. 7f) to porous and friable. The facies and mineralogic composition (calcite and/or aragonite) are controlled by water composition and temperature, CO_2 saturation and degassing rate, biotic activity, and presence of growth inhibitors (e.g., Mg/Ca ratio; Jones and Renaut 2010). Well-banded travertine can sometimes prove difficult to distinguish from epithermal carbonate vein material (Fig. 7f). However, travertine facies can contain distinctive carbonate fabrics, ranging from abiotic, shrub-like crystal forms at proximal sites to microbially influenced more distally, where stromatolites, filamentous microbial mats, and plant remains are diagnostic (e.g., Renaut et al. 2002). Travertine also commonly contains or is interbedded with iron and manganese oxides (Fig. 7f).

Travertines typically lack a close spatial relationship—and in many cases, no relationship at all—to epithermal precious metal deposits, but can occur up to several kilometers distant where they mark outflow sites of relatively cool, CO_2-rich waters. An example is provided by the tufa mounds (commonly referred to as travertine) within the moat sediments of the Creede ash-flow caldera, Colorado, which may mark the distal outflow of the Creede IS vein silver deposit (Bethke and Hay 2000). The topographically low, southeastern part of the Cerro Negro LS vein system in the Deseado massif is dominated by travertine, although there is widespread hydrothermal silicification of fissure-ridge/mound and apron travertines and stromatolitic mounds formed in the transition between subaerial and sub-lacustrine settings (Guido and Campbell 2012).

Hydrothermal chert

Chert can form where hydrothermal fluids undergo cooling as they debouch on the floors of shallow lakes, with active examples reported from the East African rift valley of Kenya (Renaut and Owen 1988). Small siliceous chimneys or spires, with or without syngenetic chert horizons (described as sub-lacustrine sinter), also formed above hot spring vents on the floors of Lake Taupo in the Taupo Volcanic Zone and Yellowstone Lake, Wyoming (de Ronde et al. 2002; Shanks et al. 2007). In principle, transitions can occur between hydrothermal chert deposits and the distal wetland facies of sinter aprons (Channing and Edwards 2013).

Hydrothermal chert, originally deposited as silica gel, can be of high purity where clastic input during its accumulation was minor, and at Stará Kremnička, Slovakia (Fig. 6b), for example, it was exploited as a raw material for manufacture of ferrosilicon alloys. There, the chert is believed to have precipitated from the distal, lower-elevation outflow from the Kremnica LS vein gold deposit, 8 km to the north (Lexa and Bartalský 1999). The chert contains fossilized marsh plants—some in growth positions, snails, frogs, and turtles, testifying to extremely shallow- and cool-water depositional conditions (Lexa and Bartalský 1999). Thinly laminated, pyritic chert also forms thin beds in the inferred hydrothermal eruption crater above the Yamada LS gold veins at Hishikari (Izawa et al. 1993) and similar material, displaying soft-sediment deformation features, occurs at the Rawhide low-grade, bulk-tonnage LS gold deposit, Nevada (Black et al. 1991).

Silicified lacustrine sediments

In rift environments conducive to LS epithermal deposit formation, silicification can be a subaqueous, syn- to diagenetic process that accompanies lacustrine sedimentation. As a result, lacustrine sediments are wholly or partly transformed to opaline silica, which eventually is recrystallized to chalcedony. The textures of the sediments, particularly fine lamination, and any contained biogenic material are commonly well preserved.

Unequivocal distinction of some sub-lacustrine, subaerial, and subsurface silicic deposits is not straightforward, even in the case of recent examples, and becomes even more difficult as a result of aging and consequent diagenetic changes (Jones et al. 2007). Silicified fine-grained lacustrine sediments and hydrothermal chert, which can be closely associated (Fig. 3), are both typically laminated, causing them to be commonly confused with one another and, potentially, also with lacustrine amorphous silica sediments. The presence of biogenic material, including plant molds, in both limnic chert and silicified sediment can further complicate their ready distinction and even their misidentification as sinter. However, silicified sediments typically have higher residual titanium contents than either limnic chert or sinter, although this compositional difference does not help to distinguish subaqueous from strata-bound subsurface silicification, which can only be accomplished on the basis of geologic context.

Silicified lacustrine sediments tend to be more widespread and abundant than either limnic chert or sinter in volcano-sedimentary rift settings, as exemplified by the Late Jurassic rift basins of the Deseado massif. The up to ~50-m-thick, strata-bound silicification in the Ivanhoe gold district took place during lacustrine sedimentation, albeit interrupted by subaerial interludes characterized by sinter deposition (Wallace 2003). However, the silicified horizon was originally interpreted as a paleogroundwater table feature, implying formation after the lake had disappeared (Bartlett et al. 1991).

Paleosurface metal contents

In contrast to the precious and base metals, which are largely immobile in a vapor at low temperatures, mercury can be transported effectively (White 1981; Barnes and Seward 1997; Christenson and Mroczek 2003), leading to its precipitation as cinnabar in the steam-heated environment. Cinnabar can also be deposited in sinters and associated opalite, either along with stibnite and other minerals from the liquid phase (e.g., Steamboat Springs, Ivanhoe, Buckskin Mountain in the National district, and Puhipuhi, North Island, New Zealand; White et al. 1964; Wallace 2003; Hampton et al. 2004; Vikre 2007) or from gases once the groundwater table has fallen. Less commonly, cinnabar impregnates mudstone laminae in hydrothermal eruption craters, as observed at Hishikari (Izawa et al. 1993) and now actively depositing at the surface of the Ngawha geothermal system, North Island, New Zealand (Ellis and Mahon 1966; Weissberg et al. 1979; Davey and van Moort 1986; Barnes and Seward 1997).

Cinnabar was formerly mined at Ngawha, from some steam-heated zones in both HS (e.g., Paradise Peak, Nevada; Sillitoe and Lorson 1994) and LS (e.g., Steamboat Springs; White et al. 1964) districts and from sinters and associated silicified rocks linked to LS deposits (e.g., McLaughlin, National, Ivanhoe, and Goldbanks districts and Puhipuhi (Lehrman 1986; White 1986; Vikre 1987, 2007; Bartlett et al. 1991; Stone et al. 2000; Fig. 8a). However, by far the largest deposits, containing corderoite ($Hg_3S_2Cl_2$) and other chloride-bearing species besides cinnabar, are hosted by opalite horizons in moat sediments of the McDermitt caldera complex, Nevada and Oregon (Rytuba and Glanzman 1979).

Although steam-heated alteration, groundwater table silicification, lacustrine amorphous silica sediments, sinter, and travertine are commonly devoid of appreciable precious- and base metal concentrations (e.g., White and Heropoulos 1983), at least at the time of initial formation, high precious metal and metalloid contents have been recorded. For example, sinters alongside the widely studied Champagne Pool, a Holocene hydrothermal eruption crater at Waiotapu in the Taupo Volcanic Zone, contain gold (up to 540 g/t) and silver (up to 745 g/t) along with thallium and mercury adsorbed onto orange-colored, amorphous arsenic and antimony sulfide precipitates (Weissberg 1969; Hedenquist and Henley 1985; Hedenquist 1986; Jones et al. 2001; Pope et al. 2005). Siliceous muds associated with a small sinter terrace along the shore of Lake Rotokawa, also in the Taupo Volcanic Zone, contain amorphous arsenic and antimony sulfides, containing elevated Au, Ag, Tl, Hg, Ga, and W; gold averages ~1 g/t (Weissberg 1969; Krupp and Seward 1987). Similar arsenic and antimony precipitates, containing up to 6500 g/t Au, some of it in telluride form, along with late-stage cinnabar occur in mudstone filling the hydrothermal eruption craters at Osorezan (Aoki and Thompson 1990; Izawa and Aoki 1991; Fig. 5b). The geochemistry of paleogroundwater table silicification is poorly characterized, although arsenic and mercury are weakly anomalous in such material at Furtei (Fig. 4d).

Sub-lacustrine hydrothermal chert is commonly anomalous in a variety of elements but not the precious metals: As, Sb, and Hg at Stará Kremnička (Lexa and Bartalský 1999) and As, Cs, Hg, Mo, Sb, Tl, and W at Yellowstone Lake (Shanks et al. 2007). Nonetheless, silicified lacustrine sediments can contain strata-bound, disseminated, precious metal mineralization, as exemplified by the Hollister LS gold-silver deposit at Ivanhoe (Bartlett et al. 1991) and San Cristóbal IS silver-zinc-lead deposit, Bolivia (Buchanan 2000; Phillipson and Romberger 2004), although many such precious metal occurrences are low-grade and remain subeconomic (e.g., Rytuba and Vander Meulen 1991a; Stone et al. 2000). Part of this sediment-hosted mineralization at San Cristóbal could be truly exhalative in origin (Buchanan 2000; Phillipson and Romberger 2004), raising the possibility of transitions between sub-lacustrine epithermal and shallow-marine

Fig. 8 Images of metal and metalloid concentrations in paleosurface products and steam-heated overprints. **a** Old Buckskin Mountain mercury workings in silicified epiclastic sediments and sinter, National LS gold district, Nevada (see Vikre 2007). **b** Gold-bearing LS vein in lacustrine mudstone overprinted by steam-heated alteration, Seta, Hokkaido, Japan. Note the porous nature of the vein quartz, resulting from carbonate and/or adularia dissolution. **c** White, powdery opaline silica (*left side*) developed during the steam-heated overprint of the alteration halo to the Paradise Peak HS gold-silver deposit, Nevada. The partly brecciated, vuggy residual quartz (*right side*), host to the orebody, was largely unaffected (see Sillitoe and Lorson 1994). **d** Cinnabar and native sulfur deposited in fractures in vuggy residual quartz during the steam-heated alteration overprint of the Paradise Peak HS gold-silver deposit, Nevada

volcanogenic massive sulfide precious metal deposits, the latter exemplified by Eskay Creek, British Columbia (Roth et al. 1999).

Precious metal mineralization can also overprint sinter in LS and IS deposits (e.g., McLaughlin; Sherlock et al. 1995) as a result of upward progradation of the underlying epithermal systems. Alternatively, steam-heated zones can overprint preexisting epithermal mineralization, leaving sufficient precious metals in the LS veins (e.g., Seta, Hokkaido, Japan; Fig. 8b) or siliceous HS ribs (e.g., Paradise Peak and Borealis, Nevada; Sillitoe and Lorson 1994; Eng 1991; Fig. 8c) for them to attain ore grade. At Hycroft, however, precious metals were reportedly stripped during formation of the steam-heated blanket, but reprecipitated in its structurally controlled roots below the then-deeper groundwater table (Ebert and Rye 1997), presumably because admixture of descendant acid-sulfate and ascendant alkali chloride waters can be an effective gold-precipitation mechanism (Reed and Spycher 1985).

Manganese and iron oxides associated with travertine are capable of scavenging a variety of metals but generally to subeconomic levels. However, a manganese oxide horizon beneath travertine at Golconda hot springs, Nevada, was formerly exploited for its tungsten content (Hewett et al. 1963). Unusually, borates (ulexite and borax) are present in some travertine deposits on the Puna plateau of northwestern Argentina (Sillitoe 1975; Alonso and Viramonte 1990).

Effects of paleosurface modification

Volcanic and geomorphologic settings

Modification of epithermal paleosurfaces and, as a direct consequence, the positions of associated paleogroundwater tables, during epithermal deposit formation can be greatly influenced by the regional-scale climatic and tectonic evolution as well as by local volcanic, structural, and geomorphologic events (Sillitoe 1993; Simmons 2002; Simmons et al. 2005).

Aggradation and progressive groundwater table ascent commonly result from the accumulation of volcanic and sedimentary material in regional- or local-scale depocenters (Fig. 9a). In contrast, erosional degradation and related groundwater table depression tend to be more common during tectonically induced uplift and attendant erosion and valley incision (Fig. 9b), climate change causing aridification (e.g., Ebert and Rye 1997), and on topographically prominent volcanic edifices. However, groundwater table descent can also be triggered almost instantaneously by volcano-related events,

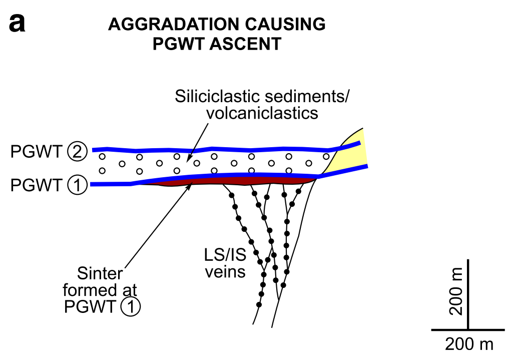

Fig. 9 Schematic sections showing effects of syn-hydrothermal aggradation and degradation in epithermal systems. **a** Burial of sinter by siliciclastic sediments and/or volcaniclastic rocks caused paleogroundwater table (PGWT) ascent from positions 1 to 2, which may have contributed to bonanza-grade development and, potentially, eventual demise of the epithermal system. **b** Valley incision caused descent of the paleogroundwater table from positions 1 to 2, thereby subjecting the sinter and rocks above paleogroundwater table 2 to steam-heated conditions; however, the sinter was little affected because of its resistant, silicic character

such as caldera formation and sector collapse, and by catastrophic drainage of lake-filled craters, calderas, and other topographic depressions (Simmons 2002; Simmons et al. 2005).

Aggradation effects

Syn-hydrothermal paleosurface aggradation can take place by accumulation of volcanic and/or sedimentary material of either local or distant provenance. Volcanic rocks can bury active epithermal systems in any volcanic setting, whereas sedimentation is most likely in the topographic depressions that characterize the extensional LS epithermal environment, but can also occur in dome complexes, ash-flow calderas, and maar volcanoes, especially under relatively pluvial climatic conditions.

Syn-hydrothermal aggradation may be relatively commonplace in the epithermal environment, but is difficult to document unambiguously unless two or more stacked sinter horizons are present, as at Hasbrouck Mountain (Graney 1987) and Verbena in the Drummond Basin, Queensland, Australia (Cunneen and Sillitoe 1989). This difficulty stems from the fact that few epithermal deposits have been discovered beneath largely barren volcanic or sedimentary cover. Even where such cover exists, it needs to be shown that its deposition was synchronous with at least the late stages of hydrothermal activity rather than accumulating later after the epithermal deposit was fully formed.

The Fruta del Norte IS gold-silver deposit provides a well-documented example of siliciclastic sedimentation over the top of a still-active epithermal system in a pull-apart basin setting (Leary et al. 2007; Fig. 10). The Fruta del Norte vein-stockwork was generated beneath a paleosurface defined by a >1-km-long sinter, which was progressively buried beneath >200 m of conglomerate and subordinate interbedded sandstone and felsic tuff (Leary et al. 2007). Confirmation that the sedimentation overlapped temporally with at least the waning stages of hydrothermal activity is provided by the presence throughout the entire conglomerate sequence of a steep, linear body of chalcedony replacement, containing

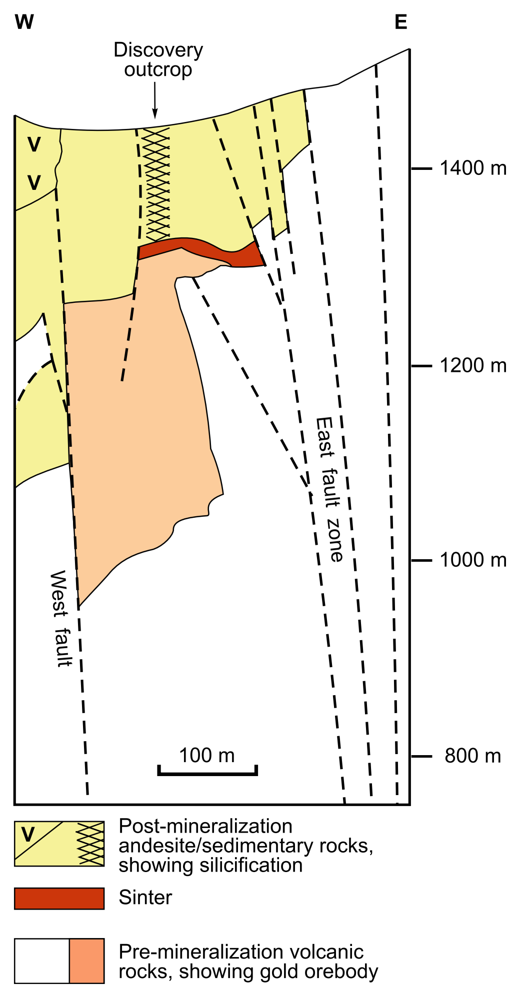

Fig. 10 Geologic section of the Fruta del Norte IS gold-silver deposit, Ecuador, showing the locations of the vein-stockwork system, overlying sinter, and silicification of the syn-hydrothermal sedimentary cover rocks (simplified from Leary et al. 2007 and unpublished data)

pyrite and marcasite, anomalous levels of arsenic and antimony, and low-order gold values (Leary et al. 2007; Fig. 10). The 40-m-thick ignimbrite flow that overlies the interpreted hydrothermal eruption crater above the Yamada veins at Hishikari is smectite altered and could also have been deposited during at least the waning stages of the epithermal system (Ibaraki and Suzuki 1993; Izawa et al. 1993).

Syn-formational burial of epithermal systems, as documented at Fruta del Norte and possibly also Hishikari, could potentially promote two competing effects. First, progressive accumulation of the overlying, water-saturated sedimentary pile could act as a partial seal, thereby favoring hydrothermal fluid entrapment and consequent precious metal grade enhancement. Second, it might eventually smother the hydrothermal system and contribute to its demise. Elsewhere, however, fine-grained fluvial and lacustrine sediments accumulating on top of epithermal systems can act as permeable hosts to low-grade epithermal deposits, as exemplified by the Hollister gold-silver orebody at Ivanhoe (Bartlett et al. 1991) and San Cristóbal silver-zinc-lead deposit.

Degradation effects

Fault-related uplift or valley incision within and nearby epithermal systems results in lowering of base level and drop of the groundwater table within the upper parts of the systems. As a result, steam-heated zones, generated above groundwater tables, can overprint previously formed paleosurface features, such as sinter and paleogroundwater table silicification as well as underlying mineralized and unmineralized rocks (Fig. 9b). Normal faulting and progressive footwall uplift caused overprinting of quartz-adularia-illite alteration by steam-heated assemblages at the Te Kopia geothermal system, Taupo Volcanic Zone (Bignall et al. 2004; Rowland and Simmons 2012). Such superposition of steam-heated alteration has also been documented at the Hycroft (Wallace 1987; Ebert and Rye 1997), Buckskin Mountain (Vikre 2007), and Florida Canyon (Fifarek et al. 2010) LS gold deposits and Arcata and Fresnillo IS silver deposits (Candiotti et al. 1990; Simmons 1991). At Arcata, the kaolinite-rich, steam-heated alteration overprinted the adularia-rich halo to the Tres Reyes vein (Fig. 4c) as well as causing dissolution of the carbonate gangue in shallow parts of the vein, leaving abundant open cavities. Although only steam-heated remnants are now present, fluid inclusion geobarometry documents syn-hydrothermal groundwater table descent of ~400 m at Fresnillo (Simmons 1991), substantially more than the 150 m at Florida Canyon (Fifarek et al. 2010) and >18 m at Hycroft (Ebert and Rye 1997). At the Cerro Millo HS prospect, Peru, a stacked series of silicified horizons has been interpreted in terms of at least 200 m of syn-hydrothermal paleogroundwater table descent (Hennig et al. 2008).

The siliceous sinter and associated silicified epiclastic deposits atop Buckskin Mountain remained largely unaffected by the paleogroundwater table descent, except for the probable introduction of cinnabar (Fig. 8a), whereas the immediately underlying rocks were transformed to steam-heated alteration assemblages (Vikre 1985, 2007). Steam-heated alteration can also overprint precious metal mineralization, hosted by either HS structures or IS and LS veins. Thus, at Paradise Peak, the steam-heated overprint introduced mercury and native sulfur to the hydrothermally brecciated, vuggy residual quartz body, which constituted the gold-silver orebody (Fig. 8d), while transforming the already-altered, flanking rocks to powdery opal-CT and opal-C (Sillitoe and Lorson 1994; Fig. 8c). Similar superposition of steam-heated alteration over auriferous siliceous ledges also appears to have taken place in parts of the Borealis HS district (e.g., Eng 1991). At the Seta prospect, an LS system associated with sinter and lacustrine sediments (Yahata et al. 1994; Yajima et al. 1997), the steam-heated alteration overprinted the shallowest quartz veins, causing them to become porous and friable (Fig. 8b).

More severe degradation of hydrothermal systems can be induced by flank or sector collapse of composite volcanoes, during which gravitational removal of up to several cubic kilometers of volcanic rock can take place in a geologic instant (Sillitoe 1994). The gravitational instability leading to flank or sector collapse commonly results from hydrothermal alteration and associated elevated fluid pressures in the summit regions and cores of the volcanoes (López and Williams 1993; Cecchi et al. 2005; Delmelle et al. 2015), but can be assisted by other processes, including volcanic and seismic activity and faulting. The hydrothermal products, including near-surface, steam-heated as well as deeper, advanced argillic assemblages that induced the edifice weakening can be observed in the resulting debris avalanche deposits (e.g., John et al. 2008). Sector collapse, massive hydrologic perturbation (e.g., volcanic eruption; Simmons et al. 2005), and other causes of abrupt groundwater table descent can cause reductions in confining pressure sufficient to produce hydrothermal brecciation and eruption as well as underlying precious metal mineralization. For example, sector collapse of a relatively small trachyandesitic stratovolcano of Pleistocene age on Lihir Island appears to have transformed incipiently developed porphyry copper-gold mineralization at depth in the volcanic edifice into the giant, near-surface, disseminated Ladolam LS gold deposit as a direct result of the decompression and consequent brecciation and fluid expulsion (Moyle et al. 1990; Sillitoe 1994; Carman 2003). Catastrophic drainage of Pleistocene glacial lakes at Yellowstone lowered the paleogroundwater table, triggering formation of at least ten hydrothermal eruption craters up to 450 m across (Muffler et al. 1971). However, as pointed out by Simmons (2002), it remains to be demonstrated that erosion by either valley incision or pedimentation is sufficiently rapid to trigger precious metal deposition, as claimed by Bissig et al. (2002, 2015) for central Andean HS gold-silver deposits.

Preservation potential

Age control

Most paleosurface features, like epithermal deposits in general (e.g., Kesler and Wilkinson 2009), tend to be relatively young, commonly Miocene or more recent, because of their susceptibility to erosional removal. Where Precambrian, Paleozoic, or Mesozoic paleosurface features are preserved, they are parts of LS or IS epithermal systems that formed beneath topographically low, extensional environments. The Devonian sinters of the Drummond Basin (Cunneen and Sillitoe 1989; White et al. 1989) and Late Jurassic sinters, travertines, and silicified lake beds of the Deseado massif (Guido and Campbell 2011), both extensional back-arc regions, are classic cases in point. Notwithstanding the existence of HS deposits of Proterozoic and Paleozoic age (e.g., Hope Brook, Newfoundland, Canada and Temora, New South Wales, Australia; Thompson et al. 1986; Dubé et al. 1998), pre-Miocene steam-heated zones in this environment are unreported because of their ease of erosional removal from volcanic centers.

Climatic control

As a generalization, arid and semi-arid regions of the world display much better preserved paleosurface features than those with pluvial climatic regimes, which explains why many of the examples of steam-heated alteration and sinter in association with epithermal deposits occur in the Great Basin of Nevada, central Andes, and Deseado massif of Patagonia. Indeed, most of the large, shallow-level HS epithermal deposits appear to be confined to the central Andean region. Paleosurface features normally only survive in Southeast Asia and the southwestern Pacific region if they are exceptionally young, as in the case of the <1-Ma and still hydrothermally active Ladolam deposit (Moyle et al. 1990; Carman 2003).

Compositional control

Many landforms on epithermal paleosurfaces are composed of soft, friable materials, as exemplified by steam-heated zones, hydrothermal eruption craters and breccias, and fossil hyperacidic lakes and mud pots. Hence, these products, as well as any associated intermediate argillic (illite-smectite) alteration zones are rapidly eroded, particularly in the pluvial climatic regimes characteristic of tropical regions, and are generally poorly preserved even in relatively young epithermal systems unless they underwent either silicification or prompt burial. For example, hydrothermal eruption craters <1800 years old in the Taupo Volcanic Zone lack topographic expression and are recognized exclusively on the basis of their distinctive and relatively restricted breccia aprons (Browne and Lawless 2001). The ephemerality of hyperacidic crater lake sediments in the HS environment may be attributed not only to their low erosional resistance but also to the extremely poor preservation potential of volcano summit regions in general.

In contrast, sinter, paleogroundwater table silicification, sub-lacustrine chert, and silicified lacustrine sediments offer much greater erosional resistance and commonly give rise to impressive examples of topographic inversion. Although formed in topographic lows, sinter, sub-lacustrine chert, and silicified lacustrine sediments can constitute topographic prominences. Arguably, the most impressive example is the late Miocene sinter and interbedded epiclastic deposits capping Buckskin Mountain, which accumulated in an intermontane basin but now cap the highest point in northern Nevada (Vikre 1987, 2007). Similarly, the Hasbrouck Mountain sinter underpins the eponymous isolated hill (Graney 1987) and the Ikiryu sinter in Kyushu, Japan, occupies a prominent, ridge-top position (Nakanishi et al. 2001). Even the erosional resistance of Holocene sinters can give rise to elevated topography (e.g., Tuhunaatara sinter, Taupo Volcanic Zone; Campbell et al. 2003). Nonetheless, many proximal sinters are largely represented by boulder fields and thinner, distal wetland facies are commonly completely destroyed (Channing and Edwards 2013). Use of the term "silica cap" for such prominent silicic features is discouraged because it fails to adequately distinguish the different silicic paleosurface landforms from one another and from deeper, strata-bound silicification.

Burial control

The simplest means of preserving paleosurface features is to quickly bury them beneath post-mineralization volcanic or sedimentary cover. Rapid syn-hydrothermal burial by sedimentary rocks accounts for the complete preservation of the Fruta del Norte IS deposit (Leary et al. 2007; see above). However, most epithermal deposits underwent at least minor erosion before concealment beneath post-mineralization units, resulting in few known examples of paleosurface features that were definitively preserved by post-mineralization volcanism or sedimentation. Arguably, the best example is provided by the Late Jurassic LS epithermal systems of the Deseado massif, which were buried and preserved beneath Cretaceous and Cenozoic continental and marine passive-margin successions (Giacosa et al. 2010). This situation is well displayed by the Cerro Negro LS vein district where any paleosurface features of hydrothermal origin were eroded prior to concealment of the shallow-level, western part of the Eureka West ore shoot beneath volcano-sedimentary rocks (Shatwell et al. 2011). Post-mineralization displacement on the normal fault that localized the Eureka West vein may have instigated the required erosion. The resultant fault scarp is flanked by talus-like breccia, containing abundant quartz vein clasts, which largely covered the outcropping vein prior to deposition of the overlying volcano-sedimentary strata.

Exploration implications

Identification of paleosurface products

The most obvious requirement for proper appreciation and, hence, successful exploration of little-eroded epithermal prospects is correct recognition of the paleosurface features present and their distinction from superficially similar, but either more deeply formed or supergene weathering products.

Steam-heated alteration needs to be distinguished from potentially ore-bearing, advanced argillic lithocap assemblages formed beneath paleogroundwater tables in HS epithermal systems (Sillitoe 1995a), which should be relatively straightforward given their distinctive textural features. The low density, presence of powdery opaline silica and alunite, and absence of residual vuggy quartz and coarsely crystalline alunite are particularly diagnostic (Table 3).

By the same token, it has to be decided if tabular silicic bodies, commonly morphologically prominent because of topographic inversion, represent chalcedonic sinter, groundwater table silicification, lacustrine amorphous silica sediments, sub-lacustrine chert beds, silicification of unconsolidated lacustrine sediments, silicified subsurface sedimentary/volcanic horizons (including jasperoid after carbonate rocks), or shallowly dipping, HS replacement ribs or crustiform IS/LS veins (Table 4; Fig. 11). Supergene sulfide oxidation causes limonite impregnation and staining of many of these silicic bodies, thereby further hindering their discrimination. The typically low precious metal contents of steam-heated alteration, groundwater table silicification, sub-lacustrine chert, and many sinters can be diagnostic, but can also lead to premature abandonment of epithermal IS and LS prospects if their true, near-surface formational sites, commonly above any precious metal concentrations, are not fully appreciated. Many of the silicic paleosurface products are characterized by an important biogenic component, although this is uncommon in the case of lacustrine amorphous silica sediments and paleogroundwater table silicification (Table 4).

Alunite and kaolinite are also widespread minerals in the surficial supergene environment and are best distinguished from their hypogene epithermal counterparts with a hand lens rather than by means of a portable spectrometer. Powdery, steam-heated and porcelanous, supergene alunites are easy

Table 3 Distinguishing features of main alunite types

Alunite type	Associated epithermal deposit type	Position	Color	Distinctive texture	Style	Relationship to epithermal mineralization	Comments
Steam heated	HS, IS, LS	Vadose zone, above groundwater table	White	Finely crystalline, friable, powdery, low density	Pervasively developed replacement blankets, up to 10-m thick; up to 70 % of rock volume	Barren unless overprinting pre-existing mineralization	Recessive weathering; low preservation potential, especially under pluvial conditions
Deep hypogene	HS	Below groundwater table	Colorless, white, cream, pink, or yellow-brown[a]	Coarse to fine crystal aggregates with quartz as massive replacements; also alone as pseudomorphs of clasts or phenocrysts and lining cavities	Steep or bedding-parallel quartz-alunite bodies, up to several 100-m thick; up to 50 % of rock volume	Sub-ore grade but anomalous in Au and Ag where massive; potentially ore-bearing where developed in hydrothermal breccias	Resistant, commonly forming prominent outcropping ribs
Supergene	HS, IS, locally LS	In oxidized zones above groundwater tables as well as in upper parts of subjacent sulfide zones; forms during active pyrite oxidation	White, cream, yellow-brown[a], or uncommonly pale green[b]	Massive, fine-grained, porcelaneous veinlets and patches; locally rock replacement	Typically occupies the youngest veinlet generation; up to 5 % of rock volume	In pyritic or formerly pyritic rocks within or beyond ore; uncommon in HS ore	Mainly developed in arid and semi-arid regions with limited groundwater recharge and dilution

[a] Due to impregnation by supergene jarosite

[b] Due to minor amounts of copper in solid solution

Table 4 Distinguishing features of flat-lying silicic products in epithermal systems

Silicic product	Associated epithermal deposit type	Areal extent	Distinctive texture(s)	Distinctive feature(s)	Contained biota	Iron sulfide content, vol %[a]
Groundwater table silicification	HS, IS, LS	Potentially extensive (<~10 km^2)	Massive, partly brecciated, with evidence of replaced lithology	Overlain by steam-heated alteration (if preserved); remanent clastic component (high Ti)	Commonly none	5–10
Amorphous silica sediments	HS, IS, LS	Relatively restricted (<~1 km^2)	Finely laminated	Soft-sediment and impact features	Commonly none, but diatoms possible	0–10
Hot spring sinter	IS, LS	Relatively restricted (<~1 km^2)	Finely laminated; geyserite, bubble-mat and/or coniform textures	Varied colors, no alteration halo	Abundant: bacteria, stromatolites, plants, pollen	Typically 0
Hydrothermal chert	IS, LS	Potentially extensive	Massive to finely laminated	Lacks appreciable clastic component (low Ti)	Abundant: subaqueous (diatoms) and subaerial	0–10
Silicified lacustrine sediments	IS, LS	Potentially extensive	Finely laminated	Remanent clastic component (high Ti)	Abundant: subaqueous (diatoms) and subaerial	5–20
Silicified subsurface horizon	HS, IS, LS	Potentially extensive	Typically massive, with evidence of replaced lithology	Overlain by clay alteration; remanent clastic component (high Ti)	Commonly none	5–20
Strata-bound jasperoid	HS, IS, LS	Relatively restricted	Variable, partly brecciated	Hosted by carbonate rock	Inherited from host limestone if present	5–30
Strata-bound replacement body	HS	Relatively restricted	Massive, texturally varied, associated vuggy residual quartz	Flanked by quartz-alunite and/or quartz-kaolinite alteration	None	10–>50
Strata-bound vein	IS, LS	Relatively restricted	Crustiform and colloform banding	Flanked by minor quartz-adularia or quartz-sericite/illite alteration	None	<5

[a] Or derivative limonite composed mainly of jarosite and/or hematite

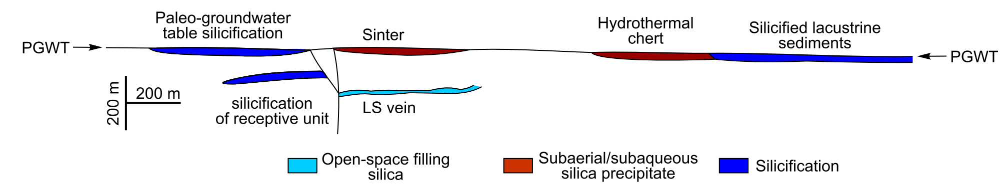

Fig. 11 Cartoon to show different types of flat-lying, surface and shallow-subsurface silicic products possible in IS and LS epithermal systems. Note that all these products can give rise to topographic inversion, resulting in their preservation as prominent surface features. Their proper distinction is one of the important keys to exploration of epithermal prospects

to distinguish from one another (Sillitoe 1993; Table 3). Rocks containing either steam-heated or supergene kaolinite are more difficult to tell apart because both, in contrast to hypogene kaolinite formed in the HS environment, normally lack associated groundmass silicification; however, the supergene variety is likely to be strongly limonitic because it is a result of pyrite oxidation. Drain-back kaolinization, formed by descendant, steam-heated waters as epithermal systems waned, also lacks accompanying groundmass silicification because the silica-bearing solutions are being heated rather than cooled.

Location of mineralization

The proximal parts of sinter aprons and terraces formed in topographically low areas, particularly where fault control of hydrothermal upflow is evident, can directly overlie LS or IS epithermal mineralization. Textures, in part imposed by the contained biota, can distinguish between near-vent and distal sinter deposits (e.g., Lynne 2012) even in old sinters, such as those of Late Jurassic age in the Deseado massif (Guido and Campbell 2014). Geyserite (Fig. 7c), providing direct evidence for boiling discharge, is a reliable indicator of proximal sinter (White et al. 1964; Campbell et al. 2015). However, where sinters lie on the lower slopes of or peripheral to volcanic edifices, such as stratovolcanoes or dome complexes, they likely formed in relatively high-temperature outflow zones, which can be distant from the potentially mineralized cores of the systems (e.g., Mac-Ban geothermal field, Philippines; Capuno et al. 2010; Fig. 1b).

Hydrothermal eruption craters and underlying breccias generally form in the proximal parts of epithermal systems and, as in the Taupo Volcanic Zone, typically mark the positions of high-flux, fluid-upflow conduits in which epithermal mineralization can be formed (Hedenquist and Henley 1985; Rowland and Simmons 2012): a situation clearly observed at Hishikari and, based on the subsurface hydrothermal vent breccia, reliably inferred at Favona (Izawa et al. 1993; Torckler et al. 2006; Figs. 3 and 6). Nonetheless, as in the case of sinters, more distal locations are also possible. Where hydrothermal eruption craters have been obliterated, recognition of eruption breccias, applying the criteria described above, including the common but by no means ubiquitous presence of at least a few vein and sinter clasts in the IS and LS environment, is critical. Increased breccia thicknesses and concentrations of large clasts can help to locate the likely sites of craters and their underlying upflow conduits (e.g., Collar and Browne 1985; Hedenquist and Henley 1985).

Where travertines are parts of epithermal systems, they are typically poor indicators of precious metal mineralization because of their characteristic distal positions relative to hydrothermal upflow zones. However, care needs to be exercised because at both Cerro Blanco and the southeastern extension of Cerro Vanguardia (Claudia), travertine and sinter are intimately related in proximity to auriferous LS veins (White et al. 2010; Guido and Campbell 2014).

Steam-heated zones and any underlying paleogroundwater table silicification can be areally extensive, locally >10 km^2, and create severe problems for explorationists. This is because surface geochemistry, most notably elevated mercury values, seems to have little direct bearing on the precise positions of underlying HS, IS, or LS epithermal mineralization. Such features are difficult to explore unless the underlying epithermal deposit has been partially unroofed by erosion, as in the case of the largely concealed Pascua-Lama HS deposit (Sillitoe 1995b), or remnants of overprinted mineralization are preserved in the steam-heated zone. Reconnaissance drill testing of large steam-heated zones that lack observable evidence for associated mineralization is best guided by an understanding of district-scale fault geometry, based on field mapping, air photograph and satellite image interpretation, and geophysical evidence. Linear, resistivity and/or non-magnetic anomalies may be particularly instructive. Nonetheless, some visually prominent and well-known steam-heated alteration zones, like that at Cuprite, Nevada, which has been used as a remote-sensing test site for the past 40 years (Swayze et al. 2014, and references therein), have so far failed to reveal the location of any underlying epithermal deposit.

Paleodepth of mineralization

Epithermal mineralization can occur in contact with or only a few meters beneath paleosurface or paleogroundwater table features, as exemplified by many epithermal deposits: HS (e.g., Yanacocha and Pascua-Lama; Harvey et al. 1999; Deyell et al. 2005), IS (e.g., Fruta del Norte; Leary et al. 2007), and LS (e.g., Hasbrouck Mountain, Ivanhoe, and McLaughlin; Graney 1987; Bartlett et al. 1991; Sherlock et al. 1995). Indeed, low-grade, bulk-tonnage HS gold ± silver deposits invariably occur in close proximity to paleosurfaces, as reliably documented by preserved erosional outliers of steam-heated alteration above most of the largest examples (Sillitoe 1999).

Nonetheless, the ore-bearing parts of some epithermal systems, especially those of IS type, occur 300–500 m and, locally, even more beneath paleosurfaces, as determined using a combination of paleogroundwater table silicification and fluid inclusion geobarometry for a number of IS vein deposits in Mexico, including the Fresnillo district (Albinson 1988; Simmons 1991). Indeed, the existence of veins at depth beneath the paleogroundwater table silicification along the western side of the Fresnillo district was predicted by Sawkins (1988) and substantiated by discovery of the Juanicipio-Valdecañas silver-gold ore shoots at a depth of ~500 m (Megaw 2010), using the data and analysis of Simmons (1991). In the National district, the tops of the LS veins are similarly deep, occurring ~270≥ 440 m beneath the sinter and interbedded silicified epiclastic rocks that cap Buckskin Mountain (Vikre 2007). The Victoria and Teresa IS veins in the Mankayan district, Philippines, must be even deeper because their tops are 150–400 m beneath the present surface (Chang et al. 2011), which, given the absence of paleosurface features, would appear to be well below the paleosurface. These appreciable gaps between paleosurface and/or paleogroundwater table features and underlying precious metal ore—commonly occupied by low-temperature, intermediate argillic alteration (mixed-layer illite-smectite and/or smectite; e.g., Chang et al. 2011)—can lead to insufficiently deep drill testing of epithermal prospects.

Similar barren or poorly mineralized gaps exist in some HS systems, as exemplified by Quimsacocha in Ecuador. There, the subhorizontal ore zone, a lithologically controlled body of highly pyritic, silicified rock, is overlain by >100 m of largely barren vuggy residual quartz cut by minor structures with locally high-grade gold mineralization (Jones et al. 2005) to which must be added an inferred, but now-eroded steam-heated blanket (Fig. 12).

A further complicating factor in the appraisal of epithermal prospects is the fact that the elevation of the tops of veins with respect to contemporaneous paleosurfaces, irrespective of whether or not paleosurface features are preserved, can vary appreciably throughout individual districts, as well illustrated by the Pachuca-Real del Monte, Mexico, and El Peñón, Chile, vein systems (Geyne et al. 1963; Warren et al. 2004; Fig. 13). Hence, although some veins may be at least partially exposed at the present surface, the nearby tops of others can lie at depths as great as 100–200 m or, in the case of Pachuca-Real del Monte, ~400 m (Fig. 13), possibly at least in part a direct result of paleogroundwater table fluctuations. Elsewhere, as demonstrated at Esquel, Argentina, widely separated, outcropping vein segments may connect at a depth beneath higher ground underlain by pre-mineralization cover rocks, implying that the original top of the vein is largely preserved (Sillitoe et al. 2002; Fig. 14). The tops of the blind veins at both Esquel and National are distinctively stibnite bearing (Vikre 1985; Sillitoe et al. 2002), in keeping with the upward concentration in epithermal systems of As, Sb, Tl, and Hg, elements that are mobile at lower temperatures (e.g., Ewers and Keays 1977; Hedenquist et al. 1996). Where all veins in a district are blind, as a result of formation beneath pre-mineralization cover, it is possible that there may have been little if any paleosurface evidence for their presence, at least vertically above them. However, hydrothermal outflow zones may be marked by low-temperature intermediate argillic alteration, travertine, and possibly, even sinter.

The fluvial and/or lacustrine sediments that accumulated syn-hydrothermally above some LS and a few IS systems are largely barren (e.g., Fruta del Norte), which poses a dilemma for explorationists who must determine if such sedimentary sequences, especially those of relatively limited areal extent, could cap blind epithermal deposits. Nonetheless, fluvio-lacustrine sequences elsewhere can contain strata-bound, disseminated orebodies (e.g., Ivanhoe, San Cristóbal). It is important though to bear in mind that bonanza-grade gold ±

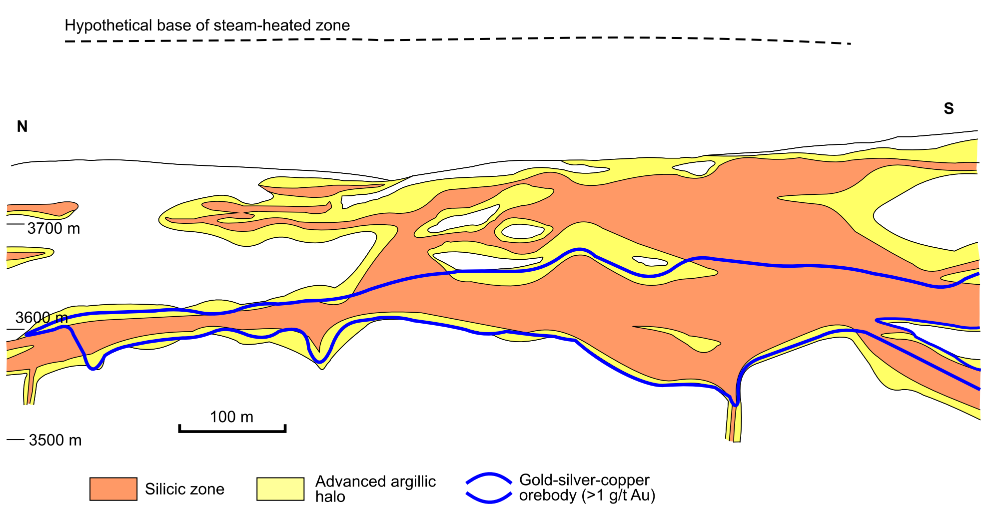

Fig. 12 Longitudinal geologic section of the volcanic rock-hosted Quimsacocha HS gold-silver-copper deposit, Ecuador, showing the subsurface position of the subhorizontal silicic orebody, which is localized by a tuffaceous horizon (taken from Jones et al. 2005). The hypothetical position of a now-eroded, steam-heated zone is also shown

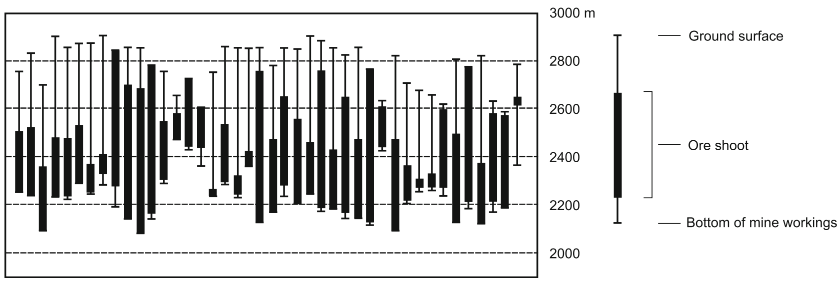

Fig. 13 Differences in original elevations of ore shoots in the Pachuca-Real del Monte IS silver-gold district, Mexico (from Geyne et al. 1963). Note that the several hundred meter elevation range of ore-shoot tops reflects differences in metal-precipitation conditions rather than post-mineralization fault displacement

silver veins can also occur at depth beneath such low-grade, disseminated mineralization, a fact only appreciated much later in the case of Ivanhoe (Tewalt 1998). This near-surface, disseminated precious metal mineralization needs to be distinguished from similarly strata-bound, but somewhat more deeply formed epithermal orebodies hosted by permeable stratigraphic units, such as the non-welded ignimbrite at the Round Mountain LS disseminated gold deposit, Nevada (Sander and Einaudi 1990), where bonanza gold grades occur in structures below, within, and above the disseminated ore (Tingley and Berger 1985).

Geochemical indicators

The precious metal contents of sinters may bear no relationship to the potential of any underlying LS or IS epithermal mineralization because, as at Champagne Pool, gold and silver are commonly scavenged by the amorphous arsenic and antimony sulfide species. Since the latter are not everywhere or continuously formed in hot springs, sinter analysis would not appear to be a particularly effective exploration technique. Nonetheless, analysis of 13 late Miocene to recent sinters from throughout Japan revealed that those associated with known gold mineralization had significantly higher average gold contents (up to 827 ppb), commonly located in proximity to hot spring vent areas and accompanied by elevated As, Sb, and Fe values (Nakanishi et al. 2003; Fig. 15). Several sinters related to LS gold deposits elsewhere have also returned broadly similar gold values (e.g., up to 1161 ppb at Buckhorn; Jennings 1991). Arsenic and antimony contents of sinters, like those of gold, can be extremely variable, but are locally extraordinarily high (e.g., up to 12,000 and 3000 ppm, respectively; Hedenquist and Henley 1985; Hayashi 2013). Furthermore, even calcite layers in the mixed silica-carbonate sinters at Savo, Solomon Islands, are enriched in As and Te (Smith et al. 2011). In conclusion, therefore, it would be reasonable to take elevated precious metal and metalloid tenors in proximal sinters as an encouraging sign of subjacent mineralization, although their absence does not necessarily condemn a prospect. Nonetheless, many sinters apparently lack associated precious metal ore at depth (e.g., McGinness Hills, Nevada and Ikiryu; Casaceli et al. 1986; Nakanishi et al. 2001).

Steam-heated zones typically also lack geochemical anomalies for precious metals and the associated element suite, other than mercury, unless they either are overprinted by or overprint precious metal mineralization, as discussed earlier. At the Purén IS silver-gold deposit, on the margin of the La

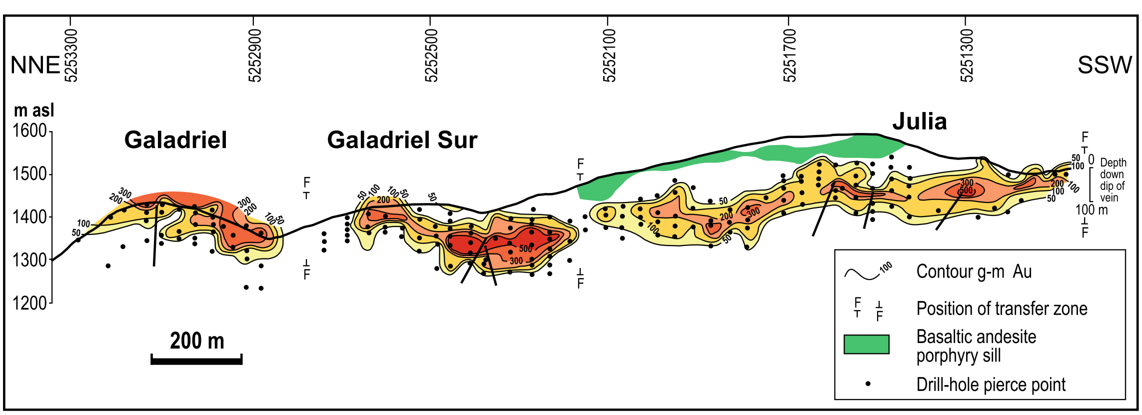

Fig. 14 Longitudinal section of the Galadriel-Julia vein at Esquel, Deseado massif, Patagonia, Argentina, showing the subsurface position of much of the LS gold-silver orebody (see Sillitoe et al. (2002) for further details). Note the presence of the basaltic andesite sill above the geologically blind portion of the Julia ore shoot

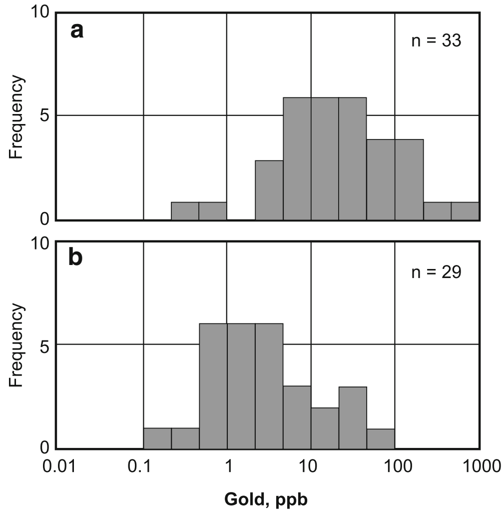

Fig. 15 Logarithmic histograms of gold contents of samples from 13 silica sinters in Japan (from Nakanishi et al. 2003). **a** Sinters associated with known gold deposits. **b** Sinters without known gold deposits. Note that the sinters associated with known gold mineralization have significantly higher gold contents, although contributions from overprinted auriferous veinlets cannot be ruled out

Coipa district, silver (up to 3 ppm) and 100×Ag/Mo (up to 17) values in steam-heated alteration define both the position and overall trend of the ore-grade, precious metal mineralization located 40 m below (Arribas et al. 2005). These low tenor silver values are inherited from pre-existing mineralization that was overprinted as a consequence of syn-hydrothermal descent of the paleogroundwater table.

The gaps between the tops of blind veins and contemporaneous paleosurfaces can be largely barren in some LS and IS epithermal systems, although low-order geochemical anomalism, typically for arsenic and antimony, may be present, especially on approach to the veins. In the case of the bonanza-grade Quebrada Colorada LS vein in the El Peñón district (Fig. 16), 100 s of ppm As and 10 s of ppm Sb extend for >100 m above its geologically blind top, although gold and silver values are insignificant (Warren et al. 2004). Similarly, the concealed Victoria IS veins, on the periphery of the Far Southeast porphyry copper-gold deposit, have up to 189 ppm As (background 0.2 ppm) at the present surface, 250–350 m above their tops (Chang et al. 2011).

Where fluvio-lacustrine sedimentation is suspected to have accompanied IS or LS epithermal activity, the recommended approach is diligent search for subtle alteration features and accompanying geochemical anomalism, particularly where faults or fractures cut the sedimentary sequences. An instructive example is provided by the structurally localized rib of silicified conglomerate situated 200 m stratigraphically above the Fruta del Norte IS deposit, which returned highly anomalous arsenic (up to several thousand ppm), antimony, and mercury values but only low-order (typically <0.3 g/t) gold values (Leary et al. 2007; Fig. 10).

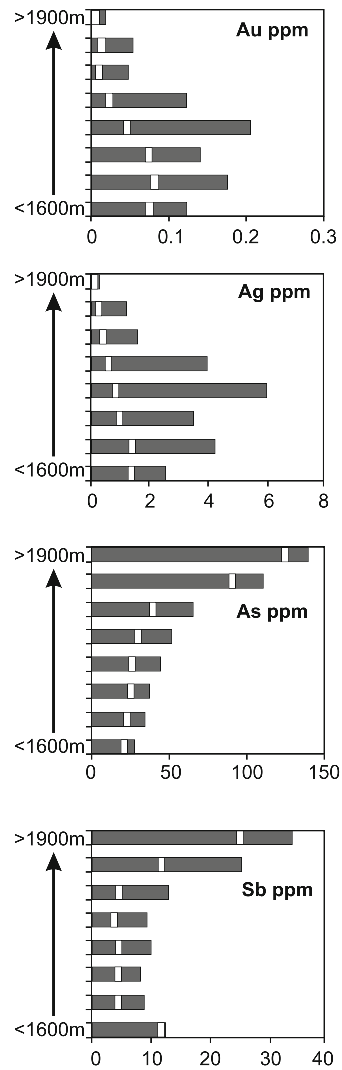

Fig. 16 Vertical geochemical gradients in rocks surrounding the Quebrada Colorada LS gold-silver vein in the El Peñón district, Chile (taken from Warren et al. 2004). *Bars* show Au, Ag, As, and Sb values averaged over 50-m intervals for drill core samples within 150 m of the vein; white bands represent median values. Note the arsenic and antimony anomalism above the geologically blind ore shoot, which has its top at ~1815 m above sea level (~80 m below surface)

Concluding remarks

Epithermal systems can be characterized by a variety of paleosurface and immediately subsurface features of great utility in the search for concealed HS, IS, and LS precious metal deposits. These features reflect district-scale hydrology, particularly the paleogroundwater table position, which may lie subsurface, at the surface or, in the location of a lake, above the surface. Distinction between these features—particularly sinter, paleogroundwater table silicification, lacustrine amorphous silica sediments, lacustrine chert, silicified fluvio-lacustrine sediments, HS silicic ribs, and IS/LS veins—all composed of superficially similar chalcedony as a result of aging and recrystallization, can facilitate understanding of epithermal districts and guide the search for concealed ore (Table 4; Fig. 11).

The shallow parts of epithermal systems undoubtedly still offer great promise for blind precious metal deposits of both bulk-tonnage disseminated and high-grade vein types. When compared to deposits concealed beneath post-mineralization cover, those beneath paleosurface features have the distinct advantage that their locations should be more readily amenable to geologic deduction. However, this advantage is somewhat limited because partial preservation of epithermal paleosurface features tends to be geographically confined to either extensional, commonly back-arc regions, characterized by semi-arid climates and relatively low erosion rates, such as the Great Basin, Mexican Altiplano, Deseado massif, and Drummond Basin, or the highly arid central Andes. Beyond such regions, where rainfall and erosion rates are higher, paleosurface remnants tend to be relatively uncommon, isolated occurrences unless the epithermal systems are either extremely young (≤1 Ma) and still at least mildly active (e.g., Cerro Blanco, Hishikari, Osorezan, Ladolam) or underwent prompt burial and relatively recent exhumation (e.g., Republic, El Dorado, Fruta del Norte, Ikiryu). Nevertheless, given the widespread existence of appreciable barren gaps between paleosurface features and tops of IS and LS veins or HS silicic replacement bodies as well as the different elevations of ore shoots in many epithermal districts, the likelihood of concealed subsurface mineralization is high even where paleosurface features have been eroded.

Acknowledgments Thanks are due to Bernd Lehmann for the invitation to prepare this paper for the 50th anniversary volume of *Mineralium Deposita*. Discussions on epithermal deposits with numerous geologists over many years, most notably Jeff Hedenquist and the late Hal Bonham, are gratefully acknowledged. The manuscript was significantly improved by the efforts of Jeff Hedenquist and Stuart Simmons and benefited from the editorial assistance of Bernd Lehmann and Georges Beaudoin. Figures 5a and 7c were kindly provided by Antonio Arribas and Stuart Simmons, respectively. This overview is dedicated to the memory of the late Hal Bonham in recognition of his contributions to the understanding of epithermal precious metal deposits in the Great Basin of Nevada.

References

Albinson T (1988) Geologic reconstruction of paleosurfaces in the Sombrerete, Colorada, and Fresnillo districts, Zacatecas State, Mexico. Econ Geol 83:1647–1667

Alonso RN, Viramonte JG (1990) Borate deposits in the Andes. In: Fontboté L, Amstutz GC, Cardozo M, Cedillo E, Frutos J (eds) Stratabound ore deposits in the Andes, SGA Spec Pub 8:721–732

Aoki M (1992) Magmatic fluid discharging to the surface from the Osorezan geothermal system, northern Honshu, Japan. In: Hedenquist JW (ed) Magmatic contributions to hydrothermal systems. Geol Surv Jpn Rep 279:16–21

Aoki M, Thompson JM (1990) The Osorezan hydrothermal system, Japan: gold-bearing hot springs. Geotherm Resour Council Trans 14:1365–1367

Arribas A, Illanes JL, Peralta C, Fuentes M (2005) Geochemical study of the steam-heated lithocap (*sic*) above the Puren deposit, La Coipa mine, Chile. In: Window to the world. Geol Soc Nevada Symposium Program with Abstracts, pp 26

Barnes HL, Seward TM (1997) Geothermal systems and mercury deposits. In: Barnes HL (ed) Geochemistry of hydrothermal ore deposits, 3rd edn. John Wiley & Sons, New York, pp 699–736

Bartlett MW, Enders MS, Hruska DC (1991) Geology of the Hollister gold deposit, Ivanhoe district, Elko County, Nevada. In: Raines GL, Lisle RE, Schafer RW, Wilkinson WH (eds) Geology and ore deposits of the Great Basin. Geol Soc Nevada Symposium Proc, vol 2, pp 957–978

Berger BR, Eimon PI (1983) Conceptual models of epithermal precious metal deposits. In: Shanks WC III (ed) Cameron volume on unconventional mineral deposits. Soc Mining Engineers, New York, pp 191–205

Bethke PM, Hay RL (2000) Overview: ancient Lake Creede. In: Bethke PM, Hay RL (eds) Ancient Lake Creede: its volcano-tectonic setting, history of sedimentation, and relation to mineralization in the Creede mining district. Geol Soc Am Spec Pap 346:1–8

Bignall G, Sekine K, Tsuchiya N (2004) Fluid-rock interaction processes in the Te Kopia geothermal field (New Zealand) revealed by SEM-CL imaging. Geothermics 33:615–635

Bissig T, Clark AH, Lee JKW, Hodgson CJ (2002) Miocene landscape evolution and geomorphologic controls on epithermal processes in the El Indio-Pascua Au-Ag-Cu belt, Chile and Argentina. Econ Geol 97:971–996

Bissig T, Clark AH, Rainbow A, Montgomery A (2015) Physiographic and tectonic settings of high-sulfidation epithermal gold–silver deposits of the Andes and their controls on mineralizing processes. Ore Geol Rev 65:327–364

Black JE, Mancuso TK, Gant JL (1991) Geology and mineralization at the Rawhide Au-Ag deposit, Mineral County, Nevada. In: Raines GL, Lisle RE, Schafer RW, Wilkinson WH (eds) Geology and ore deposits of the Great Basin. Geol Soc Nevada Symposium Proc, vol 2, pp 1123–1144

Brantley SL, Borgia A, Rowe G, Fernandez JF, Reynolds JR (1987) Poás volcano crater lake acts as a condenser for acid metal-rich brine. Nature 330:470–472

Browne PRL, Lawless JV (2001) Characteristics of hydrothermal eruptions, with examples from New Zealand and elsewhere. Earth Sci Rev 52:299–331

Buchanan LJ (2000) The geology of the San Cristobal deposit. Soc Mining Engineers Annual Meeting, Salt Lake City, Pocket Program, pp 60

Campbell KA, Rodgers KA, Brotheridge JMA, Browne PRL (2002) An unusual modern silica-carbonate sinter from Pavlova spring, Ngatamariki, New Zealand. Sedimentology 49:835–854

Campbell KA, Buddle TF, Browne PRL (2003) Late Pleistocene siliceous sinter associated with fluvial, lacustrine, volcaniclastic and landslide deposits at Tahunaatara, Taupo Volcanic Zone, New Zealand. Trans R Soc Edinb Earth Sci 94:485–501

Campbell KA, Guido D, Gautret P, Foucher F, Ramboz C, Westall F (2015) Geyserite in hot-spring siliceous sinter: window on Earth's hottest terrestrial (paleo) environment and its extreme life. Earth Sci Rev 148:44–64

Camprubí A, Albinson T (2007) Epithermal deposits in México—update of current knowledge, and an empirical reclassification. In: Alaniz-Álvarez SA, Nieto-Samaniego ÁF (eds) Geology of México: celebrating the centenary of the Geological Society of México. Geol Soc Am Spec Pap 422:377–415

Candiotti H, Noble DC, McKee EH (1990) Geologic setting and epithermal silver veins of the Arcata district, southern Peru. Econ Geol 85:1473–1490

Capuno VT, Sta. Maria RB, Minguez EB (2010) Mak-Ban geothermal field, Philippines: 30 years of commercial operation. In: World Geothermal Congress, Bali, Indonesia, 2010, Proceedings, 7 pp

Carman GD (2003) Geology, mineralization, and hydrothermal evolution of the Ladolam gold deposit, Lihir Island, Papua New Guinea. In: Simmons SF, Graham IJ (eds) Volcanic, geothermal, and ore-forming fluids: rulers and witnesses of processes within the Earth. Soc Econ Geol Spec Pub 10:247–284

Casaceli RJ, Wendell DE, Hoisington WD (1986) Geology and mineralization of the McGinness Hills, Lander County, Nevada. In: Tingley JV, Bonham HF Jr (eds) Precious-metal mineralization in hot springs systems, Nevada-California. Nev Bur Mines Geol Rep 41:93–102

Cecchi E, de Vries BW, Lavest J-M (2005) Flank spreading and collapse of weak-cored volcanoes. Bull Volcanol 67:72–91

Chang Z, Hedenquist JW, White NC, Cooke DR, Roach M, Deyell CL, Garcia J Jr, Gemmell JB, McKnight S, Cuison AL (2011) Exploration tools for linked porphyry and epithermal deposits: example from the Mankayan intrusion-centered Cu-Au district, Luzon, Philippines. Econ Geol 106:1365–1398

Channing A, Edwards D (2013) Wetland megabias: ecological and ecophysiological filtering dominates the fossil record of hot spring floras. Palaeontology 56:523–556

Christenson BW, Mroczek EK (2003) Potential reaction pathways of Hg in some New Zealand hydrothermal environments. In: Simmons SF, Graham IG (eds) Volcanic, geothermal, and ore-forming fluids: rulers and witnesses of processes within the Earth. Soc Econ Geol Spec Pub 10:111–132

Christenson BW, Wood CP (1993) Evolution of a vent-hosted hydrothermal system beneath Ruapehu Crater Lake. Bull Volcanol 55:547–565

Collar RJ, Browne PRL (1985) Hydrothermal eruptions at the Rotokawa geothermal field, Taupo Volcanic Zone, New Zealand. In: New Zealand Geothermal Workshop, 7th, University of Auckland, Proceedings, pp 171–175

Cunneen R, Sillitoe RH (1989) Paleozoic hot spring sinter in the Drummond Basin, Queensland, Australia. Econ Geol 84:135–142

Davey HA, van Moort JC (1986) Current mercury deposition at Ngawha Springs, New Zealand. Appl Geochem 1:75–93

de Ronde CEJ, Stoffers P, Garbe-Schönberg D, Christenson BW, Jones B, Manconi R, Browne PRL, Hissmann K, Botz R, Davy BW, Schmitt M, Battershill BN (2002) Discovery of active hydrothermal venting in Lake Taupo, New Zealand. J Volcanol Geotherm Res 115:257–275

de Wet CB, Davis K (2010) Preservation potential of microorganism morphologies in tufas, sinters, and travertines through geologic time. Palaeobio Palaeoenv 90:139–152

Delmelle P, Bernard A (1994) Geochemistry, mineralogy, and chemical modeling of the acid crater lake of Kawah Ijen Volcano, Indonesia. Geochim Cosmochim Acta 58:2445–2460

Delmelle P, Henley RW, Opfergelt S, Detienne M (2015) Summit acid crater lakes and flank instability in composite volcanoes. In: Rouwet D, Christenson B, Tassi F, Vandemeulebrouck J (eds) Volcanic lakes. Advances in volcanology. Springer, Berlin Heidelberg, pp 289–305

Deyell CL, Leonardson R, Rye RO, Thompson JFH, Bissig T, Cooke DR (2005) Alunite in the Pascua-Lama high-sulfidation deposit: constraints on alteration and ore deposition using stable isotope geochemistry. Econ Geol 100:131–148

Dubé B, Dunning G, Lauzière K (1998) Geology of the Hope Brook mine, Newfoundland, Canada: a preserved late Proterozoic high-sulfidation epithermal gold deposit and its implications for exploration. Econ Geol 93:405–436

Ebert SW, Rye RO (1997) Secondary precious metal enrichment by steam-heated fluids in the Crowfoot-Lewis hot spring gold-silver deposit and relation to paleoclimate. Econ Geol 92:578–600

Einaudi MT, Hedenquist JW, Inan EE (2003) Sulfidation state of fluids in active and extinct hydrothermal systems: transitions from porphyry to epithermal environments. In: Simmons SF, Graham IJ (eds) Volcanic, geothermal, and ore-forming fluids: rulers and witnesses of processes within the Earth. Soc Econ Geol Spec Pub 10:285–313

Ellis AJ, Mahon WAJ (1966) Geochemistry of the Ngawha hydrothermal area. N Z J Sci 9:440–456

Ellis J, Stroup C (2015) The Golden Devil zone, a new discovery in the Goldbanks district, Nevada. In: Pennell WM, Garside LJ (eds) New concepts and discoveries. Geol Soc Nevada Symposium Proc, vol 1, pp 663–675

Eng T (1991) Geology and mineralization of the Freedom Flats gold deposit, Borealis mine, Mineral County, Nevada. In: Raines GL, Lisle RE, Schafer RW, Wilkinson WH (eds) Geology and ore deposits of the Great Basin. Geol Soc Nevada Symposium Proc, vol 2, pp 995–1019

Ewers GR, Keays RR (1977) Volatile and precious metal zoning in the Broadlands geothermal field, New Zealand. Econ Geol 72:1337–1354

Fifarek RH, Devlin BD, Tschauder Jr RJ (1996) Au-Ag mineralization at the Golden Promise deposit, Republic district, Washington: relation to graben development and hot spring processes. In: Coyner AR, Fahey PL (eds) Geology and ore deposits of the American Cordillera. Geol Soc Nevada Symposium Proc, vol 2, pp 1063–1088

Fifarek RH, Samal AR, Miggins DP (2010) Genetic implications of mineralization and alteration ages at the Florida Canyon epithermal Au-Ag deposit, Nevada. In: Steininger R, Pennell B (eds) Great Basin evolution and metallogeny. Geol Soc Nevada Symposium Proc, vol 2, pp 861–879

Fournier RO (1983) Active hydrothermal systems as analogues of fossil systems. In: The role of heat in the development of energy and mineral resources in the northern Basin and Range province. Geotherm Resour Council Spec Rep 13:263–284

Fournier RO (1985) The behavior of silica in hydrothermal solutions. In: Berger BR, Bethke PM (eds) Geology and geochemistry of epithermal systems. Rev Econ Geol 2:45–61

Geyne AR, Fries Jr C, Segerstrom K, Black RF, Wilson IF (1963) Geología y yacimientos minerales del distrito de Pachuca–Real del Monte, Estado de Hidalgo, México. Pub Consejo Recursos Naturales no Renovables México 5E, 222 pp

Giacosa R, Zubia M, Sánchez M, Allard J (2010) Meso-Cenozoic tectonics of the southern Patagonian foreland: structural evolution and implications for Au-Ag veins in the eastern Deseado region (Santa Cruz, Argentina). J S Am Earth Sci 30:134–150

Giggenbach WF (1987) Redox processes governing the chemistry of fumarolic gas discharges from White Island, New Zealand. Appl Geochem 2:143–161

Giggenbach WF, Garcia N, Londoño A, Rodriguez L, Rojas N, Calvache ML (1990) The chemistry of fumarolic vapor and thermal-spring discharges from the Nevado del Ruiz volcanic-magmatic-hydrothermal system, Colombia. J Volcanol Geotherm Res 42:13–39

Graney JR (1987) Hasbrouck Mountain, Nevada. Precious metal mineralization in a hot springs environment. In: Johnson JL (ed) Bulk mineable precious metal mineralization of the western United States. Geol Soc Nevada Guidebook for Field Trips, pp 120–125

Guido DM, Campbell KA (2011) Jurassic hot spring deposits of the Deseado Massif (Patagonia, Argentina): characteristics and controls on regional distribution. J Volcanol Geotherm Res 203:35–47

Guido DM, Campbell KA (2012) Diverse subaerial and sublacustrine hot spring settings of the Cerro Negro epithermal system (Jurassic, Deseado Massif), Patagonia, Argentina. J Volcanol Geotherm Res 229–230:1–12

Guido DM, Campbell KA (2014) A large and complete Jurassic geothermal field at Claudia, Deseado Massif, Santa Cruz, Argentina. J Volcanol Geotherm Res 275:61–70

Guido DM, Channing A, Campbell KA, Zamuner A (2010) Jurassic geothermal landscapes and fossil ecosystems at San Agustín, Patagonia, Argentina. J Geol Soc Lond 167:11–20

Hampton WA, White GP, Hoskin PWO, Browne PRL, Rodgers KA (2004) Cinnabar, livingstonite, stibnite and pyrite in Pliocene silica sinter from Northland, New Zealand. Min Mag 68:191–198

Hancock PL, Chalmers RML, Altunel E, Çakir Z (1999) Travitonics: using travertines in active fault studies. J Struct Geol 21:903–916

Harris AC, White NC, McPhie J, Bull SW, Line MA, Skrzeczynski R, Mernagh TP, Tosdal RM (2009) Early Archean hot springs above epithermal veins, North Pole, Western Australia: new insights from fluid inclusion microanalysis. Econ Geol 104:793–814

Harvey BA, Myers SA, Klein T (1999) Yanacocha gold district, northern Peru. In: Weber G (ed) Pacrim '99 Proceedings, Bali, Indonesia, Australas Inst Min Metall, Melbourne, pp 445–459

Hayashi K (2013) Oxygen isotope study of silica sinter from the Osorezan geothermal field, northeast Japan. Int J Geosci 4:1438–1446

Hedenquist JW (1986) Waiotapu geothermal field. In: Henley RW, Hedenquist JW, Roberts PJ (eds) Guide to the active epithermal (geothermal) systems and precious metals deposits of New Zealand. Monogr Ser Min Deposits 26:65–79

Hedenquist JW (1990) The thermal and geochemical structure of the Broadlands-Ohaaki geothermal system. Geothermics 19:151–185

Hedenquist JW (1995) The ascent of magmatic fluid: discharge versus mineralization. In: Thompson JFH (ed) Magmas, fluids and ore deposits. Mineral Assoc Can Short Course Ser 23, pp 263–289

Hedenquist JW, Arribas Jr A (1999) Epithermal gold deposits: I. Hydrothermal processes in intrusion-related systems. In: Molnár F, Lexa J, Hedenquist JW (eds) Epithermal mineralization of the western Carpathians. Soc Econ Geol Guidebook Ser 31:13–34

Hedenquist JW, Henley RW (1985) Hydrothermal eruptions in the Waiotapu geothermal system, New Zealand; their origin, associated breccias, and relation to precious metal mineralization. Econ Geol 80:1640–1668

Hedenquist JW, Taran YA (2013) Modeling the formation of advanced argillic lithocaps: volcanic vapor condensation above porphyry intrusions. Econ Geol 108:1523–1540

Hedenquist JW, Aoki M, Shinohara H (1994) Flux of volatiles and ore-forming metals from the magmatic-hydrothermal system of Satsuma Iwojima volcano. Geology 22:585–588

Hedenquist JW, Izawa E, Arribas Jr A, White NC (1996) Epithermal gold deposits: styles, characteristics, and exploration. Resour Geol Spec Pub 1, 17 pp

Hedenquist JW, Arribas Jr A, Gonzalez-Urien E (2000) Exploration for epithermal gold deposits. In: Hagemann SG, Brown PE (eds) Gold in 2000. Rev Econ Geol 13:245–277

Henley RW (1985) The geothermal framework for epithermal deposits. In: Berger BR, Bethke PM (eds) Geology and geochemistry of epithermal systems. Rev Econ Geol 2:1–24

Henley RW, Ellis AJ (1983) Geothermal systems ancient and modern: a geochemical review. Earth Sci Rev 19:1–50

Hennig D, Lehmann B, Burgess R, Nekouvaght Tak MA (2008) Geology, geochemistry and $^{40}Ar/^{39}Ar$ ages of the Cerro Millo epithermal high-sulfidation gold prospect, southern Peru. Ore Geol Rev 34:304–316

Herdianita NR, Browne PRL, Rodgers KA, Campbell KA (2000) Mineralogical and textural changes accompanying ageing of silica sinter. Mineral Deposita 35:48–62

Hewett DF, Fleischer M, Conklin N (1963) Deposits of the manganese oxides; supplement. Econ Geol 58:1–51

Hochstein MP, Browne PRL (2000) Surface manifestations of geothermal systems with volcanic heat sources. In: Houghton BF, McNutt SR, Rymer H, Stix J (eds) Encyclopedia of volcanoes. Academic, San Diego, pp 835–855

Ibaraki K, Suzuki R (1993) Gold-silver quartz-adularia veins of the Main, Yamada and Sanjin deposits, Hishikari gold mine; a comparative study of their geology and ore deposits. In: Shikazono N, Naito K, Izawa E (eds) High grade epithermal gold mineralization—the Hishikari deposit. Resour Geol Spec Issue 14:1–11

Izawa E, Aoki M (1991) Geothermal activity and epithermal gold mineralization in Japan. Episodes 14:269–273

Izawa E, Naito K, Ibaraki K, Suzuki R (1993) Mudstones in a hydrothermal eruption crater above the gold-bearing vein system of the Yamada deposit at Hishikari, Japan. In: Shikazono N, Naito K, Izawa E (eds) High grade epithermal gold mineralization—the Hishikari deposit. Resour Geol Spec Issue 14:85–92

Jennings S (1991) Geology of the West Sinter deposit at the Buckhorn mine, Eureka County, Nevada. In: Raines GL, Lisle RE, Schafer RW, Wilkinson WH (eds) Geology and ore deposits of the Great Basin. Geol Soc Nevada Symposium Proc, vol 2, pp 947–956

John DA, Sisson TW, Breit GN, Rye RO, Vallance JW (2008) Characteristics, extent and origin of hydrothermal alteration at Mount Rainier Volcano, Cascades Arc, USA: implications for debris-flow hazards and mineral deposits. J Volcanol Geotherm Res 175:289–314

Jones B, Renaut RW (2010) Calcareous spring deposits in continental settings. In: Alonso-Zarza AM, Tanner LH (eds) Carbonates in continental settings: facies, environments, and processes. Dev Sediment 61:177–224

Jones B, Renaut RW, Rosen MR (2001) Biogenicity of gold- and silver-bearing siliceous sinters forming in hot (75°C) anaerobic spring-waters of Champagne Pool, Waiotapu, North Island, New Zealand. J Geol Soc Lond 158:895–911

Jones B, de Ronde CEJ, Renaut RW, Owen RB (2007) Siliceous sublacustrine spring deposits around hydrothermal vents in Lake Taupo, New Zealand. J Geol Soc Lond 164:227–242

Jones D, Barreno JE, Pérez P, Naranjo G, Viera F, Camino M (2005) The high sulphidation Quimsacocha deposit, Ecuador. In: NewGenGold 2005 conference–case histories of discovery, Perth, 2005, Proceedings. Paydirt Media Pty Ltd, West Perth, pp 119–134

Kazahaya K, Shinohara H, Saito G (2002) Degassing process of Satsuma-Iwojima volcano, Japan: supply of volatile components from a deep magma chamber. Earth Planets Space 54:327–335

Kesler SE, Wilkinson BH (2009) Resources of gold in Phanerozoic epithermal deposits. Econ Geol 104:623–633

Krupp RE, Seward TM (1987) The Rotokawa geothermal system, New Zealand: an active epithermal gold-depositing environment. Econ Geol 82:1109–1129

Kusakabe M, Hayashi N, Kobayashi T (1986) Genetic environments of the banded sulfur sediments at the Tateyama Volcano, Japan. J Geophys Res 91(B12):12159–12166

Leary S, Galarza J, Lema J, Pazmay V, Mera F, San Martin A, Santa Cruz C, Soto J (2007) The Fruta del Norte epithermal gold-silver discovery, S.E. Ecuador. In: NewGenGold 2007 conference–case histories of discovery, Perth, 2007, Proceedings. Paydirt Media Pty Ltd, West Perth, pp 113–126

Lehrman NJ (1986) The McLauglin mine, Napa and Yolo Counties, California. In: Tingley JV, Bonham HF Jr (eds) Precious-metal mineralization in hot springs systems, Nevada-California. Nev Bur Mines Geol Rep 41:85–89

Lexa J, Bartalský B (1999) Low-sulfidation epithermal gold deposit at Kremnica. In: Molnár F, Lexa J, Hedenquist JW (eds) Epithermal mineralization of the western Carpathians. Soc Econ Geol Guidebook Ser 31:265–271

Lindgren W (1933) Mineral deposits, 4th edn. McGraw-Hill Book Company, New York and London, p 930

López DL, Williams SN (1993) Catastrophic volcanic collapse: relation to hydrothermal processes. Science 260:1794–1796

Lynne BY (2012) Mapping vent to distal-apron hot spring paleo-flow pathways using siliceous sinter architecture. Geothermics 43:3–24

Lynne BY, Campbell KA, James BJ, Browne PRL, Moore J (2007) Tracking crystallinity in siliceous hot-spring deposits. Am J Sci 307:612–641

Mauk JL, Simpson MP, Hollinger E, Morrell AE, Smith N, Locke CA, Cassidy J (2006) Favona epithermal Au-Ag deposit, Waihi, Hauraki goldfield—mineralogy, geochemistry and geophysics. In: Christie AB, Brathwaite RL (eds) Geology and exploration of New Zealand mineral deposits. Australas Inst Min Metall Monogr 25: 185–190

Megaw PKM (2010) Discovery of the silver-rich Juanicipio-Valdecañas vein zone, western Fresnillo district, Zacatecas, Mexico. In: Goldfarb RJ, Marsh EE, Monecke T (eds) The challenge of finding new mineral resources: global metallogeny, innovative exploration, and new discoveries. Soc Econ Geol Spec Pub 15:119–132

Milliard JB, Marma JC, Kassos G, Hobbs E, Borchardt JS, Rehak KR (2015) Geology of the Fire Creek exploration project—low-sulfidation epithermal bonanza gold-silver deposit, Lander County, Nevada, USA. In: Pennell WM, Garside LJ (eds) New concepts and discoveries. Geol Soc Nevada Symposium Proc, vol 2, pp 1339–1364

Mongillo MA, Allis RG (1988) Continuing changes in surface activity at Craters of the Moon thermal area, Wairakei. In: New Zealand Geothermal Workshop, 10th, University of Auckland, Proceedings, pp 345–349

Moyle AJ, Doyle BJ, Hoogvliet H, Ware AR (1990) Ladolam gold deposit, Lihir Island. In: Hughes FE (ed) Geology of the mineral deposits of Australia and Papua New Guinea, vol 2. Australas Inst Min Metall Monogr 14:1793–1805

Muffler LJP, White DE, Truesdell AH (1971) Hydrothermal explosion craters in Yellowstone National Park. Geol Soc Am Bull 82:723–740

Mukaiyama H (1970) Volcanic sulphur deposits in Japan. In: Tatsumi T (ed) Volcanism and ore genesis. University of Tokyo Press, Tokyo, pp 285–294

Nairn IA, Hedenquist JW, Vilamar P, Berryman KR, Shane PA (2005) The ~AD1315 Tarawera and Waiotapu eruptions, New Zealand: contemporaneous rhyolite and hydrothermal eruptions driven by an arrested basalt dike system? Bull Volcanol 67:186–193

Nakanishi T, Taguchi S, Watanabe K, Izawa E (2001) Occurrence and structure of the Ikiryu sinter, Kuji volcanic region, north-central Kyushu, Japan. In: Feebrey CA, Hayashi H, Taguchi S (eds) Epithermal gold deposits and modern analogues, Kyushu, Japan. Soc Econ Geol Guidebook Ser 34:181–186

Nakanishi T, Izawa E, Watanabe K (2003) Mineralogical and geochemical characteristics of siliceous sinter in Japan. In: Soengkono S, Taguchi S, Simmons SF (eds) New Zealand Geothermal Workshop, 25th, University of Auckland, Proceedings, pp 155–160

Naranjo JA (1985) Sulphur flows at Latarria volcano in the North Chilean Andes. Nature 313:778–780

Nelson CE (1988) Gold deposits in the hot spring environment. In: Schafer RW, Cooper JJ, Vikre PG (eds) Bulk mineable precious metal deposits of the western United States. Geol Soc Nevada Symposium Proc, pp 417–431

Nelson CE, Giles DL (1985) Hydrothermal eruption mechanisms and hot spring gold deposits. Econ Geol 80:1633–1639

Oppenheimer C (1992) Sulphur eruptions at Volcán Poás, Costa Rica. J Volcanol Geotherm Res 49:1–21

Phillipson SE, Romberger SB (2004) Volcanic stratigraphy, structural controls, and mineralization in the San Cristobal Ag–Zn–Pb deposit, southern Bolivia. J S Am Earth Sci 16:667–683

Pope JG, Brown KL, McConchie DM (2005) Gold concentrations in springs at Waiotapu, New Zealand: implications for precious metal deposition in geothermal systems. Econ Geol 100:677–687

Rabone SDC (2006) Broken Hills rhyolite-hosted high level epithermal vein system, Hauraki goldfield—100 years on. In: Christie AB, Brathwaite RL (eds) Geology and exploration of New Zealand mineral deposits. Australas Inst Min Metall Monogr 25: 117–122

Reed MH, Spycher NF (1985) Boiling, cooling, and oxidation in epithermal systems: a numerical modeling approach. In: Berger BR, Bethke PM (eds) Geology and geochemistry of epithermal systems. Rev Econ Geol 2:249–272

Renaut RW, Owen RB (1988) Opaline cherts associated with sublacustrine hydrothermal springs at Lake Bogoria, Kenya Rift valley. Geology 16:699–702

Renaut RW, Morley CK, Jones B (2002) Fossil hot-spring travertine in the Turkana Basin, northern Kenya: structure, fabric, and genesis. In: Renaut RW, Ashley GM (eds) Sedimentation in continental rifts. SEPM Spec Pub 73:123–141

Richer M, Tosdal RM, Ullrich T (2009) Volcanic framework of the Pliocene El Dorado low-sulfidation epithermal gold district, El Salvador. Econ Geol 104:3–18

Rodgers KA, Cook KL, Browne PRL, Campbell KA (2002) The mineralogy, texture and significance of silica derived from alteration by steam condensate in three New Zealand geothermal fields. Clay Miner 37:299–322

Rodgers KA, Browne PRL, Buddle TF, Cook KL, Greatrex RA, Hampton WA, Herdianita NR, Holland GR, Lynne BY, Martin R, Newton Z, Pastars D, Sannazarro KL, Teece CIA (2004) Silica phases in sinters and residues from geothermal fields of New Zealand. Earth Sci Rev 66:1–61

Roth T, Thompson JFH, Barrett TJ (1999) The precious metal-rich Eskay Creek deposit, northwestern British Columbia. In: Barrie CT, Hannington MD (eds) Volcanic-associated massive sulfide deposits: processes and examples in modern and ancient settings. Rev Econ Geol 8:357–373

Rowe Jr GL, Brantley SL, Fernandez M, Fernandez JF, Borgia A, Barquero J (1992) Fluid-volcano interaction in an active stratovolcano: the crater lake system of Poás volcano, Costa Rica. J Volcanol Geotherm Res 49:23–51

Rowland JV, Simmons SF (2012) Hydrologic, magmatic, and tectonic controls on hydrothermal flow, Taupo Volcanic Zone, New Zealand: implications for the formation of epithermal vein deposits. Econ Geol 107:427–457

Rytuba JJ, Glanzman RK (1979) Relation of mercury, uranium, and lithium deposits to the McDermitt caldera complex, Nevada-Oregon. In: Ridge JD (ed) Papers on mineral deposits of western North America. IAGOD Quadrennial Symposium, 5th, Salt Lake City, Proceedings, vol 2. Nev Bur Mines Geol Rep 33:109–117

Rytuba JJ, Vander Meulen DB (1991a) Hot-spring precious-metal systems in the Lake Owyhee volcanic field, Oregon-Idaho. In: Raines GL, Lisle RE, Schafer RW, Wilkinson WH (eds) Geology and ore deposits of the Great Basin. Geol Soc Nevada Symposium Proc, vol 2, pp 1085–1096

Rytuba JJ, Vander Meulen DB (1991b) Field guide and road log to the DeLamar and Milestone deposits, Idaho and Oregon. In: Buffa RH, Coyner AR (eds) Geology and ore deposits of the Great Basin. Geol Soc Nevada Field Trip Guidebook and Compendium, vol 2, pp 645–655

Sander MV, Einaudi MT (1990) Epithermal deposition of gold during transition from propylitic to potassic alteration at Round Mountain, Nevada. Econ Geol 85:285–311

Sawkins FJ (1988) Anatomy of a world-class silver system, and implications for exploration. In: Jones MJ (ed) Silver—exploration, mining and treatment. Institution of Mining and Metallurgy, London, pp 33–39

Schmitt H (1950) The fumarolic-hot spring and 'epithermal' mineral deposit environment. Colo School Mines Q 45:209–229

Schoen R (1969) Rate of sulfuric acid formation in Yellowstone National Park. Geol Soc Am Bull 80:643–650

Schoen R, White DE, Hemley JJ (1974) Argillization by descending acid at Steamboat Springs, Nevada. Clay Clay Miner 22:1–22

Shanks III WC, Alt JC, Morgan LA (2007) Geochemistry of sublacustrine hydrothermal deposits in Yellowstone Lake—hydrothermal reactions, stable-isotope systematics, sinter deposition, and spire formation. In: Morgan LA (ed) Integrated geoscience studies in the greater Yellowstone area—volcanic, tectonic, and hydrothermal processes in the Yellowstone geoecosystem. US Geol Surv Prof Pap 1717:1–33

Shatwell D, Clifford JA, Echavarría D, Irusta G, Lopez D (2011) Discoveries of low-sulfidation epithermal Au-Ag veins at Cerro Negro, Deseado massif, Argentina. Soc Econ Geol Newsl 85(1):17–23

Sherlock RL, Tosdal RM, Lehrman NJ, Graney JR, Losh S, Jowett EG, Kesler SE (1995) Origin of the McLaughlin mine sheeted vein complex: metal zoning, fluid inclusion, and isotopic evidence. Econ Geol 90:2156–2181

Silberman ML, Chesterman CW (1991) A description of the Bodie Hills and Bodie mining district, Mono County, California with annotated road log from Bridgeport to Bodie. In: Buffa RH, Coyner AR (eds) Geology and ore deposits of the Great Basin. Geol Soc Nevada Field Trip Guidebook and Compendium, vol 2, pp 601–618

Sillitoe RH (1975) Lead-silver, manganese, and native sulfur mineralization within a stratovolcano, El Queva, northwest Argentina. Econ Geol 70:1190–1201

Sillitoe RH (1993) Epithermal models: genetic types, geometrical controls and shallow features. In: Kirkham RV, Sinclair WD, Thorpe RI, Duke JM (eds) Mineral deposit modelling. Geol Assoc Can Spec Pap 40:403–417

Sillitoe RH (1994) Erosion and collapse of volcanoes: causes of telescoping in intrusion-centered ore deposits. Geology 22:945–948

Sillitoe RH (1995a) Exploration of porphyry copper lithocaps. In: Mauk JL, St George JD (eds) 1995 Pacrim Congress, Auckland, Proceedings, Australasian Institute of Mining and Metallurgy, Melbourne, pp 527–532

Sillitoe RH (1995b) Exploration and discovery of base- and precious-metal deposits in the circum-Pacific region during the last 25 years. Resour Geol Spec Issue 19, 119 pp

Sillitoe RH (1999) Styles of high-sulphidation gold, silver and copper mineralisation in porphyry and epithermal environments. In: Weber G (ed) Pacrim '99 Proceedings, Bali, Indonesia, Australasian Institute of Mining and Metallurgy, Melbourne, pp 29–44

Sillitoe RH, Bonham HF Jr (1984) Volcanic landforms and ore deposits. Econ Geol 79:1286–1298

Sillitoe RH, Hedenquist JW (2003) Linkages between volcanotectonic settings, ore-fluid compositions, and epithermal precious metal deposits. In: Simmons SF, Graham IJ (eds) Volcanic, geothermal, and ore-forming fluids: rulers and witnesses of processes within the Earth. Soc Econ Geol Spec Pub 10:315–343

Sillitoe RH, Lorson RC (1994) Epithermal gold-silver-mercury deposits at Paradise Peak, Nevada: ore controls, porphyry gold association, detachment faulting, and supergene oxidation. Econ Geol 89:1226–1246

Sillitoe RH, Cooper C, Sale MJ, Soechting W, Echavarria D, Gallardo JL (2002) Discovery and geology of the Esquel low-sulfidation epithermal gold deposit, Patagonia, Argentina. In: Goldfarb RJ, Nielsen RL (eds) Integrated methods for discovery: global exploration in the twenty-first century. Soc Econ Geol Spec Pub 9:227–240

Simmons SF (1991) Hydrologic implications of alteration and fluid inclusion studies in the Fresnillo district, Mexico: evidence for a brine reservoir and a descending water table during the formation of hydrothermal Ag-Pb-Zn orebodies. Econ Geol 86:1579–1601

Simmons SF (2002) The paleosurface and paleowater table and their relationship to epithermal mineralization. Soc Econ Geol Newsl 51:28–29

Simmons SF, Brown KL (2006) Gold in magmatic hydrothermal solutions and the rapid formation of a giant ore deposit. Science 314: 288–291

Simmons SF, Browne PRL (1990) Mineralogic, alteration, and fluid-inclusion studies of epithermal gold-bearing veins at the Mt. Muro prospect, Central Kalimantan (Borneo), Indonesia. J Geochem Explor 35:63–103

Simmons SF, Keywood M, Scott BJ, Keam RF (1993) Irreversible change of the Rotomahana-Waimangu hydrothermal system (New Zealand) as a consequence of a volcanic eruption. Geology 21:643–646

Simmons SF, White NC, John DA (2005) Geological characteristics of epithermal precious and base metal deposits. In: Hedenquist JW, Thompson JFH, Goldfarb RJ, Richards JP (eds) Economic Geology One Hundredth Anniversary Volume 1905–2005. Society of Economic Geologists, Littleton, pp 485–522

Smith DJ, Jenkin GRT, Petterson MG, Naden J, Fielder S, Toba T, Chenery SRN (2011) Unusual mixed silica-carbonate deposits from magmatic-hydrothermal hot springs, Savo, Solomon Islands. J Geol Soc Lond 168:1297–1310

Stone B, Thomas D, Snider L, McDermott R, Nyman M (2000) The Goldbanks deposit, a recent discovery of disseminated gold in Tertiary volcaniclastics, Pershing County, Nevada. In: Cluer JK, Price JG, Struhsacker EM, Hardyman RF, Morris CL (eds) Geology and ore deposits 2000: the Great Basin and beyond. Geol Soc Nevada Symposium Proc, vol 1, pp 289–303

Swayze GA, Clark RN, Goetz AFH, Livo KE, Breit GN, Kruse FA, Sutley SJ, Snee LW, Lowers HA, Post JL, Stoffregen RE, Ashley RP (2014) Mapping advanced argillic alteration at Cuprite, Nevada, using imaging spectroscopy. Econ Geol 109:1179–1221

Tewalt NA (1998) Subtle surface expression of high grade veins at the Ivanhoe project. In: Kizis Jr JA (ed) Shallow expressions of deep, high-grade gold deposits. Fall 1998 Field Trip Guidebook, Geol Soc Nev Spec Pub 28:149–161

Thompson JFH, Lessman J, Thompson AJB (1986) The Temora gold-silver deposit: a newly recognized style of high sulfur mineralization in the Lower Paleozoic of Australia. Econ Geol 81:732–738

Tingley JV, Berger BR (1985) Lode gold deposits of Round Mountain, Nevada. Nev Bur Mines Geol Bull 100, 62 pp

Torckler LK, McKay D, Hobbins J (2006) Geology and exploration of the Favona Au-Ag deposit, Waihi, Hauraki goldfield. In: Christie AB, Brathwaite RL (eds) Geology and exploration of New Zealand mineral deposits. Australas Inst Min Metall Monogr 25:179–184

Trewin NH (1993) Depositional environment and preservation of biota in the Lower Devonian hot-springs of Rhynie, Aberdeenshire, Scotland. Trans R Soc Edinb Earth Sci 84:433–442

Vikre PG (1985) Precious metal vein systems in the National district, Humboldt County, Nevada. Econ Geol 80:360–393

Vikre PG (1987) Paleohydrology of Buckskin Mountain, National district, Humboldt County, Nevada. Econ Geol 82:934–950

Vikre PG (2007) Sinter-vein correlations at Buckskin Mountain, National district, Humboldt County, Nevada. Econ Geol 102:193–224

Wallace AB (1987) Geology of the Sulphur district, southwestern Humboldt County, Nevada. In: Johnson JL (ed) Bulk mineable precious metal mineralization of the western United States. Geol Soc Nevada Guidebook for Field Trips, pp 165–171

Wallace AR (2003) Geology of the Ivanhoe Hg-Au district, northern Nevada: influence of Miocene volcanism, lakes, and active faulting on epithermal mineralization. Econ Geol 98:409–424

Wallace AR, Perkins ME, Fleck RJ (2008) Late Cenozoic paleogeographic evolution of northeastern Nevada: evidence from the sedimentary basins. Geosphere 4:36–74

Walter MR, Desmarais D, Farmer JD, Hinman NW (1996) Lithofacies and biofacies of mid-Paleozoic thermal spring deposits in the Drummond Basin, Queensland, Australia. Palaios 11:497–518

Walter MR, McLoughlin S, Drinnan AN, Farmer JD (1998) Palaeontology of Devonian thermal spring deposits, Drummond Basin, Australia. Alcheringa 22:285–314

Warren I, Zuluaga JI, Robbins CH, Wulftange WH, Simmons SF (2004) Geology and geochemistry of epithermal Au-Ag mineralization in the El Peñón district, northern Chile. In: Sillitoe RH, Perelló J, Vidal CE (eds) Andean metallogeny: new discoveries, concepts, and updates. Soc Econ Geol Spec Pub 11:113–139

Watanabe T (1940) Eruptions of molten sulphur from the Siretoko-Iosan volcano, Hokkaido, Japan. Jpn J Geol Geog 17:289–310

Weissberg BG (1969) Gold-silver ore-grade precipitates from New Zealand thermal waters. Econ Geol 64:95–108

Weissberg BG, Browne PRL, Seward TM (1979) Ore metals in active geothermal systems. In: Barnes HL (ed) Geochemistry of hydrothermal ore deposits, 2nd edn. John Wiley & Sons, New York, pp 738–780

White DE (1955) Thermal springs and epithermal ore deposits. In: Bateman AM (ed) Economic Geology Fiftieth Anniversary Volume 1905–1955. Part I. Economic Geology Publishing Company, pp 99–154

White DE (1967) Mercury and base-metal deposits with associated thermal and mineral waters. In: Barnes HL (ed) Geochemistry of hydrothermal ore deposits. Holt, Rinehart and Winston, Inc, New York, pp 575–631

White DE (1973) Characteristics of geothermal resources. In: Kruger P, Otto G (eds) Geothermal energy: resources, production, stimulation. Stanford University Press, Stanford, pp 69–94

White DE (1981) Geothermal systems and hydrothermal ore deposits. In: Skinner BJ (ed) Economic Geology Seventy-Fifth Anniversary Volume 1905–1980. Economic Geology Publishing Company, pp 392–423

White GP (1986) Puhipuhi mercury deposit. In: Henley RW, Hedenquist JW, Roberts PJ (eds) Guide to the active epithermal (geothermal) systems and precious metal deposits of New Zealand. Monogr Ser Miner Deposits 26:193–198

White DE, Heropoulos C (1983) Active and fossil hydrothermal-convection systems of the Great Basin. In: The role of heat in the development of energy and mineral resources in the northern Basin and Range province. Geotherm Resour Council Spec Rep 13:41–53

White DE, Brannock WW, Murata KJ (1956) Silica in hot-spring waters. Geochim Cosmochim Acta 10:27–59

White DE, Thompson GA, Sandberg CH (1964) Rocks, structure, and geologic history of Steamboat Springs thermal area, Washoe County, Nevada. US Geol Surv Prof Pap 458-B, 63 pp

White DE, Hutchinson RA, Keith TEC (1988) The geology and remarkable thermal activity of Norris Geyser Basin, Yellowstone National Park, Wyoming. US Geol Surv Prof Pap 1456, 84 pp

White NC, Wood DG, Lee MC (1989) Epithermal sinters of Paleozoic age in north Queensland, Australia. Geology 17:718–722

White P, Ussher G, Lovelock B, Charroy J, Alexander K, Clotworthy A (2010) Mita, a newly discovered geothermal system in Guatemala. In: World Geothermal Congress, Bali, Indonesia, 2010, Proceedings, 6 pp

Wood JD (1991) Geology of the Wind Mountain gold deposit, Washoe Co., Nevada. In: Raines GL, Lisle RE, Schafer RW, Wilkinson WH (eds) Geology and ore deposits of the Great Basin. Geol Soc Nevada Symposium Proc, vol 2, pp 1051–1061

Yahata M, Kurosawa K, Ohtsu S, Takahashi T, Tomagae S, Kawamori H, Mori M (1994) Hydrothermal alteration and sedimentation at the formative period of a hot spring gold deposit: as an example of the Seta mine in Hokkaido, Japan. Resour Geol 44:1–16 (in Japanese with English abstract)

Yajima T, Matsumoto T, Koshioka K, Nakayama K (1997) Geology and exploration of the Seta low sulfidation epithermal gold deposit, eastern Hokkaido, Japan. Resour Geol 47:45–58